KSÜ Tarım ve Doğa Derg 29 (2), 265-284, 2026
KSU J. Agric Nat 29 (2), 265-284, 2026
DOI:10.18016/ksutarimdoga.vi.1734360

In Silico Prediction of Aridanin as a Potential Anticancer and Antibacterial Agent

Godloves Fru CHI[1,2✉], Yunus BAŞAR[3], Melvis Akuwen CHONGONG[4], Semiha YENIGÜN[5], Godfrey Aponglen AYIMELE[6], Ibrahim DEMIRTAŞ[7]

[1,2]https://orcid.org/0000-0002-1484-3995, [3]https://orcid.org/ 0000-0002-7785-3242, [4]https://orcid.org/0009-0002-3641-040X
[5]https://orcid.org/0000-0002-1979-5427, [6]https://orcid.org/0000-0002-1070-1236, [7]https://orcid.org/0000-0001-8946-647X

[1,6]Department of Chemistry, University of Buea, P.O. Box 63 Buea, CAMEROON, [2]Department of Pharmaceutical Chemistry, Faculty of Pharmacy, Ondokuz Mayıs University, 55139, Samsun, Türkiye, [3]Research Application Laboratories and Research Center (ALUM) Iğdır University, 76000, Iğdır, Türkiye, [4,6]Department of Chemistry, University of Bamenda, P.O. Box 34 Bambili, CAMEROON, [5]Department of Chemistry, Faculty of Science, Ondokuz Mayıs University, 55139, Samsun, Türkiye, [7]Department of Pharmaceutical Chemistry, Faculty of Pharmacy, Ondokuz Mayıs University, 55139, Samsun, Türkiye,
✉: chigodloves@yahoo.com

ABSTRACT

Aridanin, 3-*O*-[*β*-D-glucopyranosyl-(2'-acetamido)]-3*β*-olean-12-en-28-oic acid, isolated from *Tetrapleura tetraptera,* is reported to have good potential for use as an anticancer drug, especially against resistant cancers. In an *in-silico* study, the binding modes of aridanin/doxorubicin and 6 enzymes involved in cancer chemotherapy, as well as 3 antibacterial enzymes, were investigated. Also, predictions on its possible bioactivities and pharmacokinetic properties were made. Aridanin/doxorubicin enzyme interactions were determined using molecular docking and molecular dynamics simulations to attempt an explanation for its anticancer activity. Predictions of bioactivity, pharmacokinetic properties, and bioavailability scores of the molecule were calculated using PASS, SwissADME, and pKCSM. The results corroborated previous experimental data, with MolDock scores comparable to those of the standard drug and relatively higher binding energies. Accordingly, aridanin theoretically is a better inhibitor of the studied enzymes than doxorubicin. The highest inhibition recorded binding energies of -9.9, -9.2, and -10.9 kcal/mol for topoisomerase II alpha, DNA methyltransferase, and DD-peptidase, respectively. This suggests that aridanin's anticancer property may be more through interference with DNA-related proteins. In addition, ADMET/PASS anticipated that aridanin is not toxic, has a good bioavailability score of 0.56, and may display several different bioactivities. Consequently, aridanin is a potent chemotherapeutic agent against resistant cancers and bacteria that should be considered for *clinical* studies.

Biochemistry

Research Article

Article History
Received : 24.01.2025
Accepted : 16.06.2025

Keywords
Aridanin
Doxorubicin
Anticancer/Antibacterial
Molecular docking
Molecular dynamics

Aridanin'in Potansiyel Bir Antikanser ve Antibakteriyel Ajan Olarak *İn Siliko* Tahmini

ÖZET

Tetrapleura tetraptera'dan izole edilen Aridanin, 3-O-[β-D-glucopyranosyl-(2'-acetamido)]-3β-olean-12-en-28-oik asit, özellikle dirençli kanserlere karşı antikanser ilacı olarak kullanım için iyi potansiyellere sahip olduğu bildirilmiştir. Aridanin/doksorubisin ve kanser kemoterapisinde yer alan 6 enzim ve antibakteriyel 3 enzimin bağlanma modlarını değerlendirmek için bir *in siliko* çalışması yürütülmüştür. Ayrıca, olası biyoaktiviteleri ve farmakokinetik özellikleri hakkında tahminler yapılmıştır. Aridanin/doksorubisin enzim etkileşimleri, antikanser aktivitesini açıklamak için moleküler yerleştirme ve moleküler dinamik simülasyonları kullanılarak belirlenmiştir. Molekülün biyoaktivite, farmakokinetik özellikleri ve biyoyararlanım puanlarının tahminleri PASS, SwissADME ve pKCSM kullanılarak hesaplanmıştır. Sonuçlar, standart ilacınkine benzer MolDock puanları ve nispeten daha yüksek bağlanma enerjileriyle önceki deneysel verileri doğrulamıştır. Buna göre,

Biyokimya

Araştırma Makalesi

Makale Tarihçesi
Geliş Tarihi : 24.01.2025
Kabul Tarihi : 16.06.2025

Anahtar Kelimeler
Aridanin
Doksorubisin
Antikanser/Antibakteriyal
Moleküler yerleştirme
Moleküler dinamik

aridanin teorik olarak doksorubisinden daha iyi bir çalışılan enzim inhibitörüdür. En yüksek inhibisyon topoizomeraz II alfa, DNA metiltransferaz ve DD-peptidaz için sırasıyla -9,9, -9,2 ve -10,9 kcal/mol bağlanma enerjileri olarak kaydedildi. Bu, aridaninin antikanser özelliğinin daha çok DNA ile ilişkili proteinlere müdahale yoluyla olabileceğini düşündürmektedir. Ek olarak, ADMET/PASS aridaninin toksik olmadığını, 0,56'lık iyi bir biyoyararlanım puanına sahip olduğunu ve birkaç farklı biyoaktivite gösterebileceğini öngörmüştür. Sonuç olarak, aridanin klinik çalışmalar için dikkate alınması gereken dirençli kanserlere ve bakterilere karşı güçlü bir kemoterapötik ajandır.

Atıf İçin : Chi, G. F., Başar, Y., Chongong, M. A., Yenigün, S., Ayimele, G. A., & Demirtaş, I. (2026). In silico prediction of aridanin as a potential anticancer and antibacterial agent. *KSU Journal of Agriculture and Nature, 29* (2), 265-284. https://doi.org/10.18016/ksutarimdoga.vi.1623765

To Cite: Chi, G. F., Başar, Y., Chongong, M. A., Yenigün, S., Ayimele, G. A., & Demirtaş, I. (2026). Aridanin'in Potansiyel Bir Antikanser ve Antibakteriyel Ajan Olarak *İn Siliko* Tahmini. *KSÜ Tarım ve Doğa Derg, 29*(2), 265-284. https://doi.org/10.18016/ksutarimdoga.vi.1623765

INTRODUCTION

Cancer and antimicrobial resistance (AMR) are leading causes of death in the world today, necessitating a concerted effort in the search for new drugs. The importance of AMR has pushed the WHO to publish a list of pathogenic bacteria that should guide research (WHO, 2024). Plants are a rich source of molecules that are helpful in the search for new medicines. Aridanin is a lead molecule from the plant *T. tetraptera* (Schum. & Thonn) Taub., known by local names: "prekesse", "aiden fruit" or "quatre côtés", which is used as a spice in West and Central Africa (Adesina & Reisch, 1985; Anyamele et al., 2023; Mbaveng et al., 2020). The importance of this spice is evident from the great research interest bestowed on it by different groups. Previous studies have investigated the pharmacological properties of *T. tetraptera* and, in particular, aridanin and identified it as the most important compound (K. G. Sikam et al., 2022). Aridanin, 2-(N-acetyl)-D-glucopyranosyl-3β-O-olean-12-en-28-oic acid, a major compound from *T. tetraptera* is a derivative of oleanolic acid reported to have *in vivo* anticancer properties (Gupta, 2022). In previous studies, aridanin exhibited interesting pharmacological properties, including anticancer (Mbaveng et al., 2020), cytotoxicity (Mbaveng et al., 2020; Zheng et al., 2021), antibacterial (Kamdem Kengne et al., 2022), antiproliferative (Tang et al., 2022; Zhang et al., 2021), molluscidal (Adesina et al., 2016; Taiwo et al., 2018), anxiolytic (Aderibigbe et al., 2011), among others. Nevertheless, this molecule has not attracted enough attention from pharmaceutical companies, clinicians, and drug developers to explore its potential further. One of the reasons for this lack of interest is the fact that triterpenes are considered promiscuous in terms of their activity, and their mode of action is not well understood. Inhibition of enzymes is one of the mechanisms by which drugs get rid of pathogens. Cancer is a major cause of mortality worldwide (Siegel et al., 2023) and therefore requires a constant search for new and affordable medicines, especially for people with modest incomes. According to (Chhikara & Parang, 2022), around 10 million people die of cancer every year. Consistent efforts are therefore required to develop new therapeutics. Several enzymes play an important role in different stages of cancer, including proliferation, invasion, metastasis, and angiogenesis. Key enzymes in cancer metabolism include: Topoisomerase II alpha, p53, Bcl-52, DNA methyltransferase I, Her2, mdm2, interleukins, aminopeptidase N, ribonucleotide reductase (Bandyopadhyay et al., 2018). A molecule with the ability to inhibit one, some or all of these enzymes is a potential anticancer drug (Bandyopadhyay et al., 2018). As a continuation of our interest in this important molecule, the potential of aridanin as an anticancer drug candidate is highlighted here by demonstrating its enzyme-inhibitory activities using computational methods, which may make it more attractive for further anticancer drug development research. Molecular docking is a structure-based drug design method commonly used to assess the 3D orientation of molecules at a receptor site (Brogi et al., 2020) and to quantify the interactions between the atoms of the molecule and the receptor. This is important because it reduces costs by limiting the fields of experimentation. The interaction between aridanin and nine different enzymes is investigated by molecular docking, molecular dynamics simulations, and binding energy calculations in comparison to the standard anticancer drug doxorubicin, and its pharmacokinetic properties are determined. For a molecule to be effective as a drug, it must reach the target in sufficient concentration and remain there long enough in a bioactive form to achieve the expected biological effects (Daina et al., 2017). This is assessed in drug development by evaluating the absorption, distribution, metabolism, excretion, and toxicity (ADMET) of a molecule. SwissADME is a free web tool widely used in the evaluation of pharmacokinetics, drug likeness, and medicinal chemistry of small molecules (Daina et al., 2017). The standard cancer drug doxorubicin (DOX) is an anthracycline antibiotic that was first extracted from *Streptomyces peucetius* var. *caesius* and is used effectively against a range of cancers

(Meredith & Dass, 2016). The use of DOX has been limited by its severe side effects and toxicity during or after treatment (Micallef & Baron, 2020). In our previous study, we reported that the aridanin molecule has anti-cancer properties. In this study, the interactions of the aridanin molecule with anticancer (DNA topoisomerase II, alpha, P53, BCL-2, DNA methyltransferase 1, Her2, Mdm2) and antibacterial (DNA gyrase, glucosamine-6-phosphate and DD-peptidase) enzymes were theoretically determined by molecular docking and molecular dynamics simulations. In addition, the pharmacological properties of aridanin were determined by PASS, SwissADME, and pKCSM applications. In this way, the inhibitory properties and pharmacological effects of the aridanin molecule are determined, and information on its suitability as a drug candidate is provided.

MATERIAL and METHOD

Extraction and Isolation of Aridanin:

The fruit pods of *T. tetraptera* were collected from Dschang in March 2018. They were authenticated at the National Herbarium (Yaoundé, Cameroon), where voucher specimens were kept as 12117/SRFCam. The crushed fruits (1230 g) were macerated three times in dichloromethane-methanol (CH_2Cl_2-MeOH; 1:1; 10 L) for 48 hours and then filtered. The filtrate was evaporated under vacuum to obtain 188.65 g of a dark brown paste. The paste was separated by a solid-liquid method into the fractions hexane (5.0 g), ethyl acetate (20.3 g), MeOH (82.24 g), and a residue of 45.69 g. The residue was dissolved in water and extracted with n-BuOH to obtain 40.22 g of the n-BuOH fraction. The n-BuOH fraction of *T. tetraptera* (38.23 g) was dissolved in $CHCl_3$-MeOH (1:1 v/v, 100 mL) and absorbed onto 50.00 g of fine silica gel, mounted on a silica gel column packed with 338.0 g of fine silica gel and eluted with $CHCl_3$-MeOH gradient (100:0, 98:2, 95:5, 93:7, 90:10, 85:15, 80:20, 75:25, 70:30). 320 fractions of 200 mL each were collected and pooled into TtB1 (1 – 42), TtB2 (43 – 88), TtB3 (89 – 168), TtB4 (169 – 221), TtB5 (222 – 249), and TtB6 (250 – 320) according to their TLC profiles. Compound 1 (120 mg) was obtained directly from the silica gel column of fraction TtB4 (subfraction 180 – 200) eluted with $CHCl_3$-MeOH (93:7, 90:10, 85:15) and cleaned by gel filtration on Sephadex LH20 using $CHCl_3$-MeOH (70:30).

Cytotoxicity

The cytotoxic potential of aridanin against 18 cancer cells, including sensitive and drug-resistant phenotypes mediated by P-glycoprotein, BCRP, p53 knockout, EGFR deletion mutations, or BRAF mutations, was investigated. In addition, the mechanism of aridanin-induced cell death in metastatic B16/F10 cells, HepR2 hepatocarcinoma, and normal AML12 hepatocytes was investigated. The resazurin reduction assay was used to evaluate cytotoxicity, autophagy, ferroptotic, and necroptotic cell death in CCRF-CEM leukemia cells (Mbaveng et al., 2021).

Enzyme selection criteria

The enzymes used for this study were selected following two main criteria: in addition to being mentioned as targets in common forms of cancer, their action should be against tumor DNA or RNA (Espinosa et al., 2003). Enzymes that contribute to DNA synthesis and enzymes involved in DNA replication could be targets in common forms of cancer, such as breast, prostate, lung, liver, and colon. Disruption of the activity of the DNA-related protein topoisomerase II alpha, which is involved in DNA replication, transcription, and chromosome segregation, leads to enzyme-mediated DNA damage (Kumar et al., 2015; Lin, 2016). Some drugs act by forming inter-strand cross-links that alter the DNA structure and function, commonly known as alkylating agents. The high concentration of DNA methyltransferase I in the S phase of the cell cycle makes it a specific target for the inhibition of methylation in rapidly dividing cells - a characteristic feature of cancer. Methylation directly affects DNA alkylation to covalent bonds with the bases in DNA, hence preventing replication (Zhang et al., 2022). Some anticancer molecules act against specific mRNAs such as bcl-2, p53, mdm2, Her-2, and methyltransferase-1. These are usually targeted with molecules such as oligonucleotides (Kumar et al., 2015; Wang et al., 2024). Inhibition of p53 or its negative regulator MDM2, by any molecule, will lead to cell cycle arrest or apoptosis in p53-positive stressed cells (Hafezi & Rahmani, 2021; Marvalim et al., 2023). Overexpression of MDM2 and loss of p53 function were identified in different cancer types, including lung, liver, breast, esophageal, gastric, colorectal cancers, as well as sarcomas, melanoma, leukemia, lymphoma, and globlastoma (Wang et al., 2024; Yoshino et al., 2006; Zhao et al., 2014). Targeting anti-apoptosis proteins of the BCL-2 family can promote apoptosis and thus overcome the resistance of tumors to chemotherapy (Qian et al., 2022; Yoshino et al., 2006). HER-2 receptors on the surface of breast cancer cells can be blocked by other molecules (drugs), preventing them from receiving growth signals, leading to cell death. DNA gyrase is an essential enzyme in all prokaryotic cells and a good target for antibacterial agents (Spencer & Panda, 2023). Other common antibacterial enzymes are glucosamine-6-phosphate (Wojciechowski et al., 2005) and DD-peptidase (Kohanski et al., 2010). DD-peptidase is involved in cell wall

synthesis, and inhibition will weaken the cell wall, like penicillin.

Molecular docking application

The 3D structures of aridanin and standard doxorubicin were drawn in the ChemDraw Professional 2019 application, and the minimum energy was calculated and saved in SYBL2 and MDL Molfile formats. The enzymes 3D X-ray structure of selected for this docking study were anti-cancer enzymes; DNA topoisomerase II, alpha [PDB ID: 1ZXM, resolution: 1.87 Å], P53 [PDB ID: 1YCR, 2.60 Å], BCL-2 [PDB ID: 2W3L, 2.10 Å], DNA methyltransferase 1[PDB ID: 3AV6, 3.09 Å], Her2 [PDB ID: 3PP0, 2.25 Å], Mdm2 [PDB ID: 4SCJ, 2.30 Å], DNA gyrase [PDB ID: 1KZN, 2.30 Å], glucosamine-6-phosphate [PDB ID: 1MOQ, 1.57 Å] and DD-peptidase [PDB ID: 3PDE, 1.75 Å] in protein data bank (PDB). The interactions between aridanin/doxorubicin and enzymes were determined using the Molegro Virtual Docker (MVD) program (Başar et al., 2024; Namba-Nzanguim et al., 2024). The enzymes and aridanin were added to MVD, and 5 independent runs (poses) were performed using the directed differential evolution algorithm, returning each enzyme and aridanin. The score for the best pose was recorded according to the MolDock scoring function used by MVD. 2D and 3D images of the interactions were created (BIOVIA Discovery Studio Visualizer). The binding affinities of aridanin with enzymes were calculated by AutoDock Vina (Başar & Karadağ, 2024; Başar et al., 2025; Yenigun et al., 2024a, 2024b).

MD Simulations and MM-PBSA Analysis

The graphical representations of root-mean-square deviation (RMSD), radius of gyration (Rg), root-mean-square fluctuation (RMSF), and hydrogen bonds of aridanin interaction with the enzymes with the highest activity were revealed by MD simulations (GROMACS software). The MD simulation was conducted using the CHARMM force field in July 2022. TIP3P water was used to solvate the complexes and the unbound enzyme after they were put in a tricyclic box. The system's overall charge was neutralized by the addition of Na^+ and Cl^- ions. To save energy, 50,000 steps were then taken using the steepest decline technique. Then, using NVT/NPT, the system's pressure and temperature were adjusted to 100 kPa and 310 K, respectively. Lastly, a hundred nanoseconds of MD simulation were run (Gok et al., 2025). The MD simulations were optimized to 100 ns, and the diagrams were created using GRACE software. The free binding energy of the protein-ligand complex was determined using the Molecular Mechanics/Poisson-Boltzmann surface area (MM/PBSA) method. The tool "g_mmpbsa" was used to obtain the free energies of binding for each complex (Başar et al., 2025; Chi et al., 2025; Kumari et al., 2014).

Prediction of Activity Spectra for Substances (PASS)

The PASS analysis to determine the bioactivity spectrum of aridanin was performed on the PASS online web server (http://www.pharmaexpert.ru/passonline) (Lagunin et al., 2000). The PASS prediction can be used to predict various biological activities (with an accuracy of 90%). This method compares the probability that a substance is active (Pa) with the probability that it is inactive (Pi) using the simplified molecular line entry system (SMILES). Activities for a particular chemical are only accepted if Pa>Pi. The values of Pa and Pi vary between 0.000-1.000, and since they are calculated separately, Pa+Pi≠1. According to the PASS prediction, it has a higher activity when Pa>0.7 and a lower activity when Pa≤0.5 (Chi et al., 2025; Yenigün et al., 2024c).

Pharmacokinetic properties (ADMET) determination

Pharmacokinetic properties and bioavailability scores of the aridanin molecule were estimated on SwissADME (https://www.swissadme.ch/) and pKCSM (Daina et al., 2017; İpek et al.). ADMET is a method for understanding and predicting the effects of drugs on the human body. Aridanin structure (2D) from Chemdraw Professional 2019 was imported into SwissADME web page and prompted to output 49 properties used to describe the molecule's drug likeness. Seventeen of these descriptors include physicochemical properties: molecular weight (MW), number of H-bond acceptors (nHA), number of H-bond donors (nHD), number of rotatable bonds (nRB); solubility (Log P, Log S,); pharmacokinetics: gastrointestinal absorption (GIa), blood-brain barrier permeability (BBBp), P-glycoprotein (P-gp), skin permeability (Log Kp); Drug properties: lipinski, total clearance (CLtot), absorption in human intestine (IA), steady-state volume distribution (VDss), oral acute toxicity (LD_{50}), cytochrome substrate (CYP), bioavailability score. These parameters are discussed further for Aridanin in the ADMET is an important application to improve treatment options, reduce adverse events, and improve clinical trials.

RESULTS and DISCUSSION

Identification of aridanin

Aridanin was isolated from $CHCl_3$ – MeOH (93:7, 90:10, 85:15) subfractions as a white powder, m.p. 276.8 – 277.3°C, sparingly soluble in methanol and very soluble in DMSO. Its molecular mass, 659.4392, was obtained

from HRESIMS, and the molecular formula, $C_{38}H_{61}NO_8$ (Calcd: 659.4397) determined in corroboration with data from 1D & 2D NMR (Table 1). The structure of aridanin was determined by analyzing its spectrometric data and comparing it with data from the literature (Adesina & Reisch, 1985; K. G. Sikam et al., 2022). The relative configuration *β-* was assigned to C-3 on the basis of NOESY correlations: H-3/H-24 and H-3/H-25 (Figure 1).

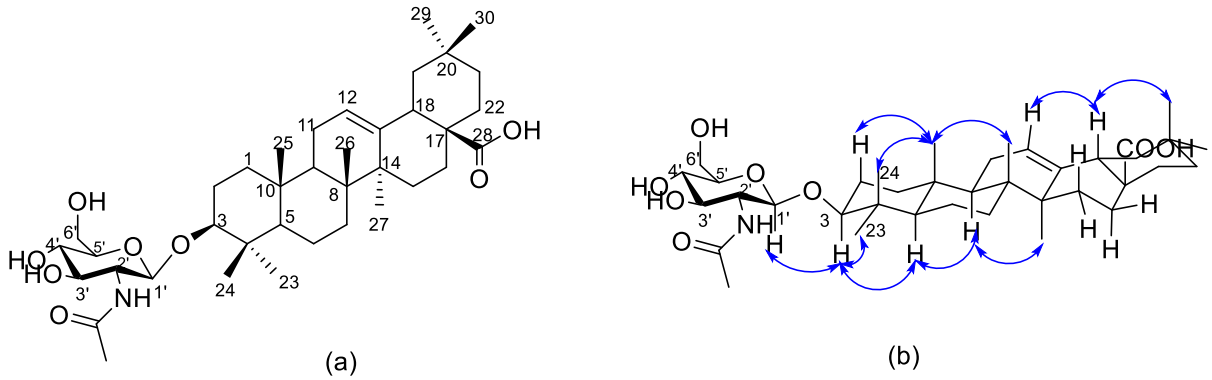

Figure 1. (a) structure of Aridanin, (b) NOESY correlations for Aridanin congener.
Şekil 1. (a) Aridanin yapısı, (b) Aridanin konjenerinin NOESY korelasyonları.

Thus, the compound was named as 3-*O*-[(2'-acetamido)-*β*-D-glucopyranosyl]-3*β*-olean-12-en-28-oic acid, white amorphous powder; $[\alpha]_D^{25}$ + 17.1 (MeOH, c 1.00); IR (KBr) υ_{max} cm^{-1}: 3433, 2939, 1695, 1645, 1524, 1463, 1366, 1167, 1074, 1026, 670; for ^1H, ^{13}C spectroscopy data, see table 1, *m/z* 659.4392 was obtained from HRESIMS and the molecular formula, $C_{38}H_{61}NO_8$ (Calcd: 659.4397).

Cytotoxicity of Aridanin

Aridanin and the positive control, doxorubicin, inhibited the proliferation of all 18 cancer cells tested. The IC_{50} values varied between 3.18 µM (CCRF-CEM cells) and 9.56 µM (HepG2 cells). Aridanin had significantly lower IC_{50} values than the standard drug doxorubicin against multidrug-resistant CEM/ADR5000 cells and melanoma cell lines: MaMel-80a, Mel-2a, MV3, and SKMel-505. Aridanin has been shown to induce apoptosis in CCRF-CEM cells through increased reactive oxygen species, degradation of mitochondrial membrane potential, and, to a lesser extent, through activation of caspases (Mbaveng et al., 2020). Based on the interesting inhibitory activity *in vitro*, we studied the *in silico* inhibitory activities in order to set a base for further *in vitro* and clinical studies.

Molecular Docking

Interactions of Aridanin and Doxorubicin with topoisomerase II alpha

Aridanin interacted with topoisomerase II alpha by forming five conventional hydrogen bonds to amino acid TRP62, LYS83, GLN310, GLU379, GLN309, three carbon bonds with amino acid ARG242, GLN309, ALA318, one pi-sigma with amino acid TYR82, five alkyls to amino acid bonds with ILE311, ALA318, LEU238, and four pi-alkyls with amino acid TRP62, TYR82, PHE308, PHE313 (Figure 1-Table 1). The MolDock score for Aridanin in topoisomerase II alpha was determined to be -121.32, with a corresponding binding energy of -9.9 kcal/mol (Table 1).

The interaction of doxorubicin with topoisomerase II alpha was via four conventional hydrogen bonds to amino acid TYR72, ARG241, GLN310, GLN309, six carbon hydrogen bonds to amino acid ILE311, SER320, GLN309, GLN60, TYR82, three alkyls to amino acid MET61, and four pi-alkyls to amino acid TYR82, ALA318, ILE311 (Figure 2 -Table S2). MolDock score of -93.90 was deduced for the interaction of doxorubicin and topoisomerase II alpha with binding energy -7.4 kcal/mol (Table 1).

Interactions of Aridanin and Doxorubicin with p53

The interactions of the aridanin molecule with p53, shown in Figure S10-Table S3, through four conventional hydrogen bonds with amino acids LYS51, GLU28, TRP23; four carbon-hydrogen bonds with amino acids PHE55, TRP23, GLU28; two alkyls to amino acids LYS24, MET62; and two pi-alkyls to amino acid PHE55. A MolDock score of -88.41, binding energy of -7.6 kcal/mol was computed for aridanin interaction with p53 (Table 1).

Doxorubicin interaction in the active site of p53 (Figure S11-Table S4) was via four conventional hydrogen bonds to amino acids GLN59, LYS51, LEU26, LEU54; four carbon hydrogen bonds with amino acids LYS51, TRP23, GLU28; two pi-cations with amino acid LYS24, two t-shaped pi-pi to amino acid PHE55; and two pi-alkyls to the

amino acid LYS24. The MolDock score -77.51, and binding energy -7.0 kcal/mol (Table 1) were determined for Doxorubicin-p53 interaction.

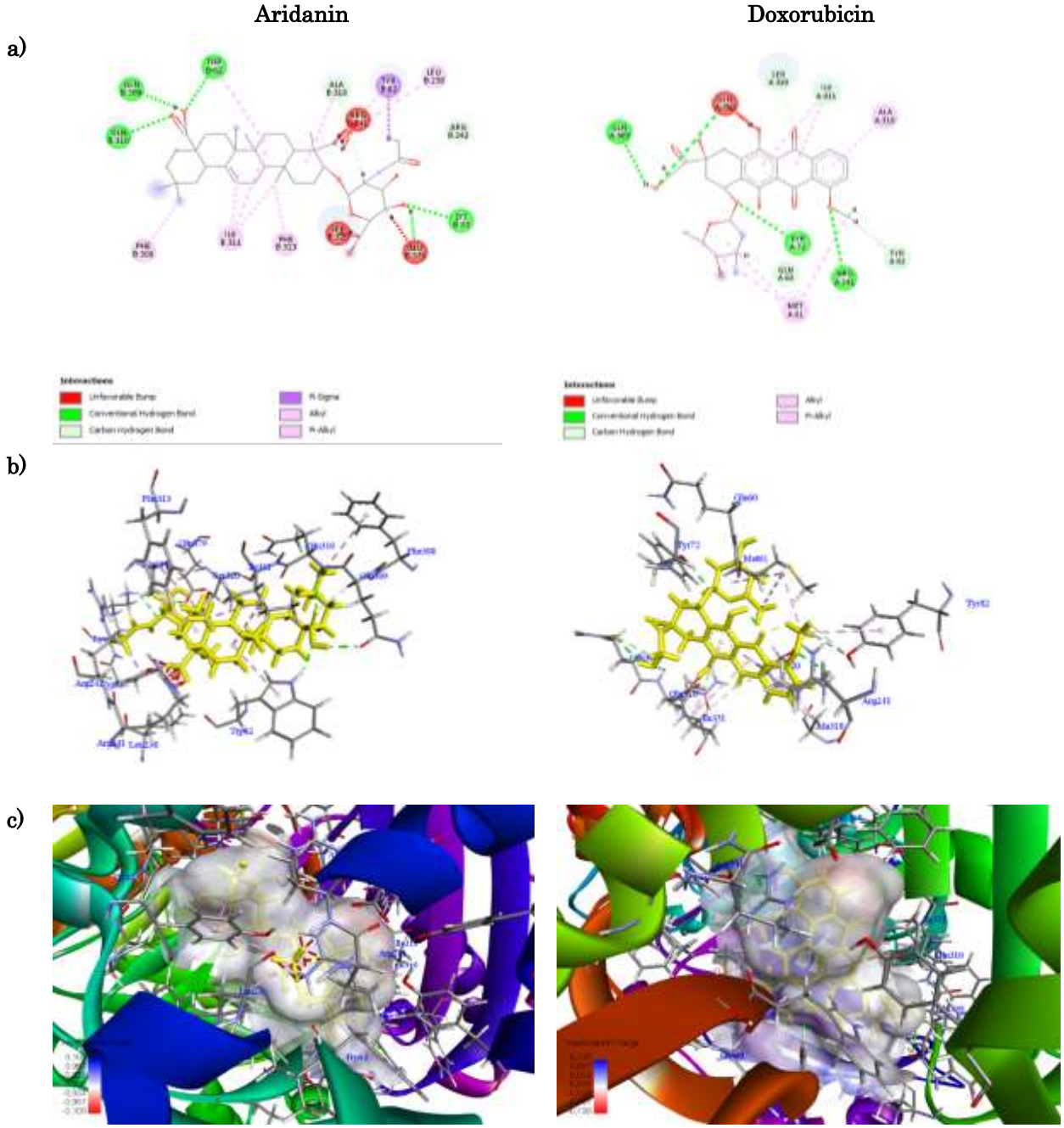

Figure 2. Interaction of Topoisomerase II alpha isoenzymes with aridanin a) 2D image b) general view c) Interpolated load 3D view.

Şekil 2. Topoizomeraz II alfa izoenzimlerinin aridanin ile etkileşimi a) 2B görüntü b) genel görünüm c) Ara yük 3B görünümü.

Interaction of Aridanin and Doxorubicin with bcl-52

Aridanin molecule interacted with bcl-52 by five conventional hydrogen bonds to amino acids LEU59, GLU135, GLN118, GLU136, eight carbon hydrogen bonds to amino acids GLU135, GLU136, THR132, GLN118, fourteen alkyls with amino acids LEU119, VAL133, LYS58, LEU59, VAL133, LEU119, ARG129, and one pi-alkyl to amino acid PHE153 (Figure S11-Table S5). Aridanin with bcl-52 MolDock score of -122.00 and binding energy -8.1 kcal/mol was determined as in Table 1.

Table 1: ^{1}H NMR (600 MHz, DMSO), ^{13}C NMR (151 MHz, DMSO), COSY, NOESY, HSQC and HMBC correlation for aridanin compared to similar data in the literature (Adesina and Reisch, 1985; Sikam *et al.*, 2023).

Çizelge 1: Aridanin için 1H NMR (600 MHz, DMSO), 13C NMR (151 MHz, DMSO), COSY, NOESY, HSQC ve HMBC korelasyonu literatürdeki benzer verilerle karşılaştırılması (Adesina and Reisch, 1985; Sikam et al., 2023).

No	Compound 1 (aridanin)					(Adesina et al., 1985)	(Sikam et al., 2022)
	^{1}H δ (ppm)	^{13}C δ (ppm)	HMBC	COSY	NOESY	^{13}C δ (ppm)	^{13}C δ (ppm)
	1.49 (m, 1H), 0.86 (m, 1H)	37.98	16.29, 36.23, 38.33, 54.87			38.5	38.5
	1.78 (m, 1H), 1.48 (m, 1H)	25.26	15.06, 36.23, 37.98, 54.87, 88.02	2.96 (H-3)		26.2	26.2
	2.96 (dd, *J* = 11.6, 4.5 Hz, 1H)	88.02	16.29, 25.26, 27.53, 38.33, 103.52	1.48 (H-2)	0.64 (H-24), 0.84 (H-25)	89.1	89.1
		38.33				39.1	39.1
	0.68 (d, *J* = 1.8 Hz, 1H)	54.87	16.29, 17.75, 36.28			55.7	55.7
	1.42 (m, 1H), 1.26 (m, 1H)	17.75				18.4	18.4
	1.38 (m, 1H), 1.21 (m, 1H)	32.36	17.75, 38.85, 47.03, 54.87			33.2	33.2
		38.85				39.6	39.6
	1.48 (m, 1H)	47.03	15.06, 16.26, 36.28, 38.85, 41.28			47.9	47.9
		36.28				36.9	36.9
	1.79 (m, 1H) 1.46 (m, 1H)	22.59	15.06, 16.26, 27.07, 36.28, 38.85, 45.67			23.6	23.6
	5.14 (t, *J* = 3.7 Hz, 1H)	121.49	22.88, 25.52, 40.78, 41.28, 45.43, 47.03	1.79 (H-11)	2.73 (H-18)	122.3	122.3
		143.81				144.7	144.7
		41.28				42.1	42.1
	1.63 (m, 1H), 0.97 (m, 1H)	27.16				28.1	28.1
	1.90 (td, *J* = 13.5, 4.0 Hz, 1H), 1.46 (m, 1H)	22.59	27.16, 178.52			23.7	23.7
		45.67				46.6	46.6
	2.73 (dd, *J* = 13.9, 4.7 Hz, 1H)	40.78	22.59, 45.43, 121.49, 143.81, 178.56	1.56 (H-19)		41.9	41.9
	1.56 (m, 1H), 1.04 (ddd, *J* = 13.5, 4.8, 2.2 Hz, 1H)	45.67		2.73 (H-18)		46.4	46.4
		30.38				30.9	30.9
	1.47 (m, 1H)	33.28				34.1	34.1
	1.31 (m, 1H), 1.13 (m, 1H)	33.28	30.38,			33.2	33.2
	0.88 (s, 3H)	27.53	16.29, 38.33, 54.87, 88.02			28.1	28.1
	0.64 (s, 3H)	16.29	27.53, 38.33, 54.87, 88.02	1.27 (H-)	1.49 (H-1), 0.84 (H-25)	16.9	16.9
	0.84 (s, 3H)	15.06	36.28, 37.98, 47.03, 54.87		0.64 (H-24)	15.4	15.4
	0.70 (s, 3H)	16.26	32.36, 38.85, 41.28, 47.03			17.3	17.3
	1.08 (s, 3H)	25.52	27.16, 38.85, 41.23, 143.81			26.1	26.1
		178.52				180.1	180.1
	0.86 (s, 3H)	32.81	23.32, 30.38, 33.28, 45.67			33.2	33.2
	0.86 (s, 3H)	23.35	30.38, 32.81, 33.28, 45.67	1.47		23.7	23.7
1'	4.24 (d, *J* = 8.4 Hz, 1H)	103.52	55.82, 74.00, 76.67, 88.02	3.39	2.96 (H-3), 3.27 (H-3')	104.7	104.7
2'	3.39 (m, 1H)	55.82		7.68		58.0	58.0
3'	3.27 (ddt, *J* = 9.9, 7.4, 3.8 Hz, 1H)	74.00	76.67, 168.69, 103.52			76.0	76.0
4'	3.03 (*br*s, 1H)	70.72				72.6	72.6
5'	3.03 (*br*s, 1H)	76.67	70.72, 76.67			78.0	78.0
6'	3.64 (m, 1H), 3.42 (dd, *J* = 10.2, 4.5 Hz, 1H)	61.16	70.2	3.42, 3.63		62.9	62.9
$CH_3\underline{C}O$		168.69				170.2	170.2
$\underline{CH_3}CO$	1.77 (m, 3H)	23.10				23.6	23.6
$\underline{H}$ – N	7.68 (d, *J* = 9.2 Hz, 1H)	-		3.39	1.77 ($C\underline{H_3}$-), 3.27 (H-3')		

While doxorubicin formed eight conventional hydrogen bonds with GLU179, GLU135, HIS184, THR122, six carbon hydrogen bonds with amino acids TRP176, ARG183, HIS184, TRP176, two pi-cations with amino acids ARG183, one pi-sigma with amino acid HIS184, and one pi-alkyl with amino acid HIS184 in the active site of bcl52 (Figure S11-Table S6). A MolDock score of -86.24, binding energy of -7.4 kcal/mol was determined for doxorubicin bcl-52 interactions (Table 1).

Interaction between Aridanin, Doxorubicin, and DNA methyltransferase 1

Aridanin molecule interacted with DNA methyltransferase 1 via four conventional hydrogen bonds to amino acids CYS1151, GLN1230, PHE1148, ASP1146: seven carbon hydrogen bonds with amino acids GLY1150, GLY1225, GLU1269, SER1149, PHE1148, ASN1580, SER1149, and five alkyls with amino acid VAL529, VAL1271, VAL1582, PRO1228 (Figure S11-Table S7). A MolDock score of -125.96 and binding energy of -9.2 kcal/mol were computed for aridanin-DNA methyltransferase 1 interactions (Table 2).

On the other hand, the Doxorubicin-DNA methyltransferase 1 interaction formed five conventional hydrogen bonds with amino acids GLY1226, VAL1582, ASN1580, ASP1146, six carbon hydrogen bonds with amino acids PHE1148, GLY1226, PRO1227, GLU1269, SER1149, a pi-anion interaction with amino acid GLU1171, a pi-sulphur with amino acid MET1172, an amide-pi stacked with PRO1227, two alkyls to ALA1581, MET1172, and five pi-alkyls with PHE1148, PRO1228 amino acids (Figure S11-Table S8). A MolDock score of -130.26 and binding energy -8.1 kcal/mol (Table 2) was deduced for Doxorubicin-DNA methyltransferase 1 interactions.

Interactions between Aridanin, Doxorubicin, and her2

Aridanin's interactions with her2 are recorded in Table 2. It formed six conventional hydrogen bonds to amino acids LYS765, LYS957, ASP769, ARG966, and two carbon hydrogen bonds with amino acids CYS965, ASP769, and six alkyl links to amino acids LYS65, LYS957, PRO967, ILE954 PRO1228 (Figure S11-Table S9). A MolDock score of -115.92 and binding energy of -8.2 kcal/mol were determined for aridanin-her2 interactions, as in Table 2. Doxorubicin-her2 interactions occurred via seven conventional hydrogen bonds to TYR772, ILE872, ARG978, ARG985, ASP838, ASP950 amino acids, two carbon bonds with amino acids ASP769, LEU768, three stacked pi-pi stacked interactions to TYR772 amino acid, four alkyls to VAL773, VAL839, LEU869, MET953 amino acids, and three pi-alkyl to TYR772 and MET953 amino acids (Figure S11-Table S10). Doxorubicin-her2 interactions had a MolDock score of -90.64 and binding energy of -8.0 kcal/mol (Table 2).

Interaction between Aridanin, Doxorubicin, and mdm2

Aridanin-mdm2 interacted via 4 conventional hydrogen bonds with LYS60, HIS72, SER32 amino acids, 2 carbon-hydrogen bonds interactions with amino acids SER36, ASN75, and 7 alkyls with LYS60, PRO77, LYS35, PRO28, LEU31 amino acids (Figure S11-Table S11). A MolDock score of -106.82 and binding affinity of -7.8 kcal/mol were deduced for Aridanin-mdm2 interactions (Table 2).

Doxorubicin-mdm2 interacted via 5 conventional hydrogen bonds to amino acids: TYR56, LYS60, LEU29, SER32; 3 carbon hydrogen bonds with amino acid SER32, LEU29, ASP76, six alkyls with amino acid LEU29, LEU33, LEU81, LYS60, PRO77, and two pi-alkyls with amino acid LYS35 (Figure S11-Table S12). Doxorubicin with mdm2 was calculated as a MolDock score of -68.95, with binding energies of -7.0 kcal/mol (Table 2).

Interactions of Aridanin and Doxorubicin with DNA Gyrase

The aridanin-DNA gyrase interaction forms 2 conventional hydrogen bonds with amino acids VAL43, VAL71, and ASN46, 3 carbon hydrogen bonds to amino acids THR165, VAL71, and 3 alkyl to amino acid PRO79 (Figure S11-Table 13). Aridanin - DNA gyrase complex had a MolDock score -97.94 and a binding affinity of -7.10 kcal/mol (Table 2).

Doxorubicin - DNA gyrase complex formed 8 conventional hydrogen bonds with amino acids GLY77, THR165, ASP73, VAL43, VAL71, GLU50, a carbon hydrogen bond with amino acid VAL71, pi-donor hydrogen bond to the amino acid ASN46, 4 alkyls with amino acids VAL43, VAL12, VAL167, ILE90, and a pi-alkyl with the amino acid ILE78 (Figure S11-Table 14). Doxorubicin - DNA gyrase complex recorded a MolDock score -96.91 and binding energies -7.00 kcal/mol (Table 2).

Interactions of Aridanin and Doxorubicin with Glucosamine-6-phosphate

Aridanin - glucosamine-6-phosphate interacted by; 6 conventional hydrogen bonds with amino acids THR352, CYS300, GLN348, SER303, SER349, LYS603, 3 carbon hydrogen bonds to amino acids CYS300, LYS603, 6 alkyls to amino acids LYS487, LEU601, ALA602, VAL605, LEU484 (Figure S11-Table 15). Aridanin - Aridanin-

glucosamine-6-phosphate complex had a MolDock score -110.55 and binding affinity -8.30 kcal/mol (Table 2).

Doxorubicin - glucosamine-6-phosphate interacted through: 9 conventional hydrogen bonds with amino acids CYS300, SER303, SER349, SER401, LYS603, ALA602, GLU488, SER347, 8 carbon hydrogen bond with amino acids SER303, SER347, SER401, VAL399, SER303, THR352, VAL605, ASP354, amide-pi stacked with amino acid CYS300, alkyl with amino acid CYS300, VAL605 and pi-alkyl to amino acids CYS300, VAL605 (Figure S11-Table 16). Doxorubicin-glucosamine-6-phosphate complex recorded a MolDock score of -96.60 and binding affinity of -6.30 kcal/mol (Table 2).

Interactions of Aridanin and Doxorubicin with DD-peptidase

The aridanin - DD peptidase interacted via 4 conventional hydrogen bonds with the amino acids ARG285, ASN327, GLN303, THR123, a carbon-hydrogen bond with the amino acid ASN327, an alkyl bond with the amino acid LEU332, and 4 pi-alkyl bonds with the amino acids PHE320, TRP233 (Figure S11-Table S17). The aridanin - DD-peptidase complex had a MolDock score of -121.68 and a binding affinity of -10.90 kcal/mol.

Doxorubicin - DD-peptidase complex we held by 4 conventional hydrogen bonds with amino acids ASN61, GLN303, THR123, 2 carbon hydrogen bonds with amino acid ASN117, a t-shaped pi-pi interaction with amino acid PHE120, and a pi-alkyl to amino acid TRP233, as on Figure S11 and Table S18. A MolDock score of -89.87 and binding affinity of -8.70 kcal/mol was determined for Doxorubicin - DD-Peptidase complex.

Table 2. MolDock score and binding energy values of Aridanin and Doxorubicin molecules.
Çizelge 2. Aridanin ve Doksorubisin moleküllerinin MolDock skoru ve bağlanma enerjisi değerleri.

Enzymes	Aridanin		Doxorubicin	
Anticancer	**MolDock score**	**Binding energy (kcal/mol)**	**MolDock score**	**Binding energy (kcal/mol)**
Topoisomerase II, alpha	-121.32	-9.9	-93.90	-7.4
P53	-88.41	-7.6	-77.51	-7.0
Bcl-52	-122.00	-8.1	-86.24	-7.4
DNA methyltransferase 1	-125.96	-9.2	-130.26	-8.1
Her2	-115.92	-8.2	-90.64	-8.0
Mdm2	-106.82	-7.8	-68.95	-7.0
Bacteria				
DNA gyrase	-97.94	-7.1	-96.91	-7.0
Glucosamine-6-phosphate	-110.55	-8.3	-96.60	-6.3
DD-peptidase	-121.68	-10.9	-89.87	-8.7

The results for molecular docking are summarized in Table 3, while detailed interactions are recorded in Tables S1-S16. The MolDock scores of aridanin with anticancer enzymes were determined as -121.32 (topoisomerase II alpha), -88.41 (P53), -122.00 (Bcl-52), -125.96 (DNA methyltransferase I), -115.92 (Her2), and -106.82 (Mdm2). The MolDock scores of the interactions of doxorubicin with the same enzymes were recorded as -93.90, -77.51, -86.24, -130.26, -90.64, and -68.95, respectively. In the molecular docking created with DNA methyltransferase I in anticancer enzymes, both aridanin and the drug had high MolDock score values.

The binding affinities of aridanin are -9.9 kcal/mol (topoisomerase II alpha), -7.6 kcal/mol (P53), -8.1kcal/mol (Bcl-52), -9.2 kcal/mol (DNA methyltransferase I), -8.2 kcal/mol (Her2), -7.8 kcal/mol (Mdm2), while the binding affinities of doxorubicin are -7.4 kcal/mol (topoisomerase II alpha), -7.0 kcal/mol (P53), -7.4 kcal/mol (Bcl-52), -8.1 kcal/mol (DNA methyltransferase I), -8.0 kcal/mol (Her2), -7.0 kcal/mol (Mdm2). According to these binding affinity results, it was determined that aridanin had high affinity in molecular docking with topoisomerase II alpha, while the drug was also highly active in DNA methyltransferase I.

When the MolDock scores and binding affinities of the enzymes in bacteria with aridanin were examined, it was calculated as -97.94 and -7.1 kcal/mol (DNA gyrase), -110.55 and -8.3 kcal/mol (glucosamine-6-phosphate), -121.68 and -10.9 kcal/mol (DD-peptidase), while the MolDock scores and binding affinities of doxorubicin were calculated as -96.91 and -7.0 kcal/mol (DNA gyrase), -96.60 and -6.3 kcal/mol (glucosamine-6-phosphate), -89.87 and -8.7 kcal/mol (DD-peptidase). As can be understood from these results, the highest effect was observed in the DD-peptidase enzyme.

In Fig. 2, a portion of Fig. S11, showing Aridanin / Doxorubicin interactions with enzymes captured as a 2D image, general, and 3D interpolated load view. Generally, doxorubicin formed more H-bonds than aridanin, however, the MolDock score for aridanin was comparable to that of doxorubicin, though slightly higher in most cases. Secondly, the binding energies of aridanin with enzymes were relatively higher than those for doxorubicin-enzyme. This may

suggest that aridanin is a comparable anticancer agent to doxorubicin, as confirmed by one of our previous investigations on this molecule (Mbaveng *et al.*, 2020a). The highest binding energies of -9.9, -9.2, and -10.9 kcal/mol were recorded for topoisomerase II alpha, DNA methyltransferase 1, and DD-peptidase, respectively, suggesting that the molecule hinders most DNA-related proteins. Aridanin may be a better anticancer agent in that it forms less strong H-bonds to the enzymes, as does doxorubicin, which could be the reason for the toxicity registered with doxorubicin (Chen et al., 2018; Lao et al., 2013).

MD Simulation and MM-PBSA Analysis

Molecular dynamics (MD) is employed to study the dynamic behavior of complex systems where atoms and molecules interact over time (Liu et al., 2018). Any effective computational analysis of a molecule in the drug development quest must consider the MD of the molecule in question. MD simulations consider the targets' flexibility in contrast to conventional molecular docking methods, in which the molecule is somewhat rigid. In this sense, binding energy estimations can predict potential inhibitors more precisely (Liu et al., 2018). MD modelling is essential for comprehending proteins' dynamic processes and conformational changes (Decherchi & Cavalli, 2020). Molecular drug design, material science, biophysics, and the nutritional mechanisms of biological macromolecules, according to (Rapaport, 2004) are all established via MD simulations. This is in line with the induced-fit model, which holds that both enzyme and substrate undergo dynamic conformational changes upon binding. Thus, when a protein interacts with an external substance, the active site modifies the protein's structure and energy (6). MD simulation was used to study aridanin's impact on the 1ZXM (Topoisomerase II), 3AV6 (DNA methyltransferase 1), and 3PTE (DD-peptidase) proteins from both structural and energetic points of view (Elkaeed et al., 2022; Yousef et al., 2022). Accordingly, MD simulations helped to forecast the dynamics and stability of aridanin with 1ZXM, 3SV6, and 3PTE in physiological settings (Rehman et al., 2019).

The protein's conformational stability was assessed by calculating the scalar distance between its C backbone and its throughput trajectory using the protein-ligand complex's root-mean-square deviation (RMSD). Greater RMSDs showed that the proteins' backbone changed structurally during the simulation period, whereas lower RMSD values suggested that the protein was highly stable. RMSD plot taken for 100 ns, for the aridanin-1ZXM complex of the protein-ligand complexes, a 5 nm RMSD value was observed in the ranges of 10-20 ns, 30-40 ns, and 70-90 ns, while it was observed between 5-15 nm for the other parts. For the aridanin-3AV6 complex, it was observed that it varied between 0.3-0.9 nm for 100 ns but remained constant at 0.8 nm after 40 ns. For the aridanin-3PTE complex, it was observed that it remained stable at 8 nm throughout the simulation. These results show that the 3PTE complex is more stable (Fig. 3a, 4a, and 5a).

The root-mean-square fluctuation (RMSF) method was used to compute variations in each amino acid residue in the presence and absence of distinct ligand molecules during the simulation process. The fluctuation intensity persisted between 0.05-0.5 nm, 0.1-1.2 nm, and 0.05-0.35 nm, respectively, according to the RMSF, computed for all complex systems using the Cα atoms of 1ZXM, 3AV6, and 3PTE (Fig. 3b, 4b, and 5b). In contrast to 1ZXM and 3AV6, 3PTE shows lower RMSF values, suggesting that aridanin binding aids in structural stabilization and decreases enzyme flexibility. The proteins' structure stability and the presence of flexible areas required to achieve the optimal conformations were therefore determined by the RMSF plots.

To determine the stability of the ligand-receptor complex, it was essential to investigate the bonding interactions between proteins and ligands throughout the MD simulations (Majewski et al., 2019). Figs. 3c, 4c, and 5c display the H-bond formed by ligand, 1ZXM, 3AV6, and 3PTE during 100 ns MD simulations. For the aridanin-1ZXM, aridanin-3AV6, and 3PTE complexes, the bonds between six to eight H-bonds continuously interacted over the MD simulation period.

The radius of gyration (Rg) indicates how compact a protein is. Rg is an effective and relevant indicator to assess the ability of a drug to change the structure of proteins. The Rg value provides information about the loose molecular packing of a protein. Fig. 3d illustrates how the dynamics computation for 100 ns showed that the aridanin-1ZXM was seen to be constant at around 2.7 and 0.5 nm. The dynamics computation for 100 ns demonstrated that the aridanin-3AV6 was consistent at approximately 3.6 and 0.5 nm (Fig. 5d). Furthermore, the dynamics computation for 100 ns demonstrated that the 3PTE and aridanin were consistent at approximately 2.0 and 0.5 nm (Figure 6d). A molecule with a high Rg is more elongated or has a wider spatial dispersion, which often denotes a more unfolded or less compact shape. On the other hand, a molecule with a low Rg is more compact, which often denotes a structure that is more folded or densely packed. In contrast to 1ZXM and 3AV6, 3PTE has lower Rg values, suggesting that aridanin binding stabilizes the 3PTE enzyme and encourages a more compact, folded shape.

One of the most popular techniques for determining binding free energy is MM-PBSA. A ligand-protein complex is predicted to be more stable and have better ligand activity and potency when its predicted binding free energy is

lower. MM-PBSA measured protein-ligand complexes' binding free energy (ΔGbinding). As can be shown in Figure 6 and Table 3, the RA's ΔGbinding values are -16.74±12.02, -25.89±7.11, and -22.94±5.21 kcal/mol for 1ZXM, 3AV6, and 3PTE, respectively. The output parameters of the MD simulation correlate well with the docking results, which demonstrate that docked protein-ligand complexes stay stable during the simulation. As a result, the MD output parameters matched the docking output parameters, indicating that the docked protein-ligand complex remained stable during the simulation.

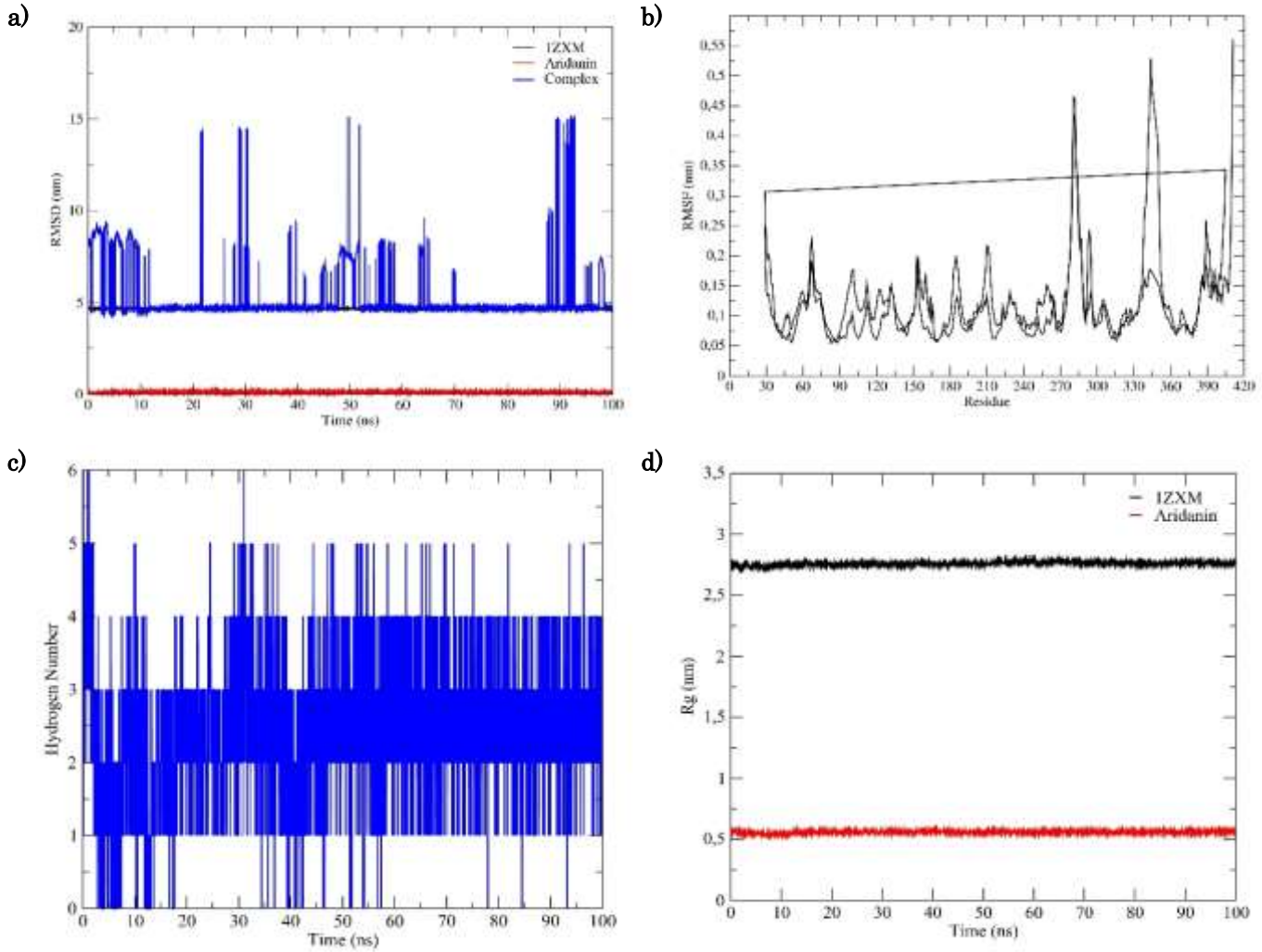

Figure 3. RMSD (a) RMSF (b) variations of the backbone within MD trajectories for peptides and the complex, time-dependent H-bond interactions (c), and Rg plotting (d) with 1ZXM.

Şekil 3. RMSD (a) RMSF (b) peptitler için MD yörüngeleri içindeki omurganın değişimleri ve karmaşık, zamana bağlı H-bağı etkileşimleri (c) ve 1ZXM ile Rg çizimi (d).

Table 3. Results for MM/PBSA determination of Energies of Aridanin (kcal/mol).
Çizelge 3. Aridanin Enerjilerinin (kcal/mol) MM/PBSA ile belirlenmesine ilişkin sonuçlar.

Enzymes	VDW (kcal/mol)	EEL (kcal/mol)	EGB (kcal/mol)	E_{SURF} (kcal/mol)	ΔG_{GAS} (kcal/mol)	ΔG_{SOLV} (kcal/mol)	$\Delta G_{Binding}$ (kcal/mol)
1ZXM	-34.79±23.68	-10.95±9.04	33.79±23.03	-4.79±3.26	-45.74±31.38	29.00±19.81	-16.74±12.02
3AV6	-49.19±3.84	-20.70±9.53	50.62±6.45	-6.62±0.48	-69.89±10.92	44.00±6.24	-25.89±7.11
3PTE	-39.08±5.45	-10.27±7.79	31.60±8.19	-5.20±0.90	-49.35±11.52	26.41±7.49	-22.94±5.21

VDW: van der Waals contribution, EEL: electrostatic energy as calculated by the MM force field, EGB: the electrostatic contribution to the free solvation energy as calculated by GB, Esurf: hydrophobic contribution to the free solvation energy for GB calculations, ΔGGAS: total gas phase energy (ELE + VDW + INT), ΔGsolv: sum of non-polar and polar contributions to solvation, ΔGBinding: binding free energy (kcal/mol).

Prediction of Activity Spectrum for Aridanin

A series of biological activities of aridanin were predicted using PASS online analysis. The activity probability (Pa) and inactivity probability (Pi) of the analysis are shown in Table 4. In the PASS analysis, the experimental probability of activity is higher when Pa>0.7. Accordingly, aridanin has high caspase 3 stimulant,

hepatoprotectant, chitinase inhibitor, membrane integrity antagonist, CDP-glycerol glycerophosphotransferase inhibitor, caspase 8 stimulant, immunostimulant, wound healing agent, chemopreventive, transcription factor NF kappa B stimulant, transcription factor stimulant, antiviral (influenza), antiprotozoal (leishmania), antiulcerative, antineoplastic, oxidoreductase inhibitor, lipid peroxidase inhibitor, alpha glucosidase inhibitor, antinociceptive, DNA ligase (ATP) inhibitor, apoptosis agonist, insulin promoter, aspartyl transferase inhibitor and hepatic disorders treatment.

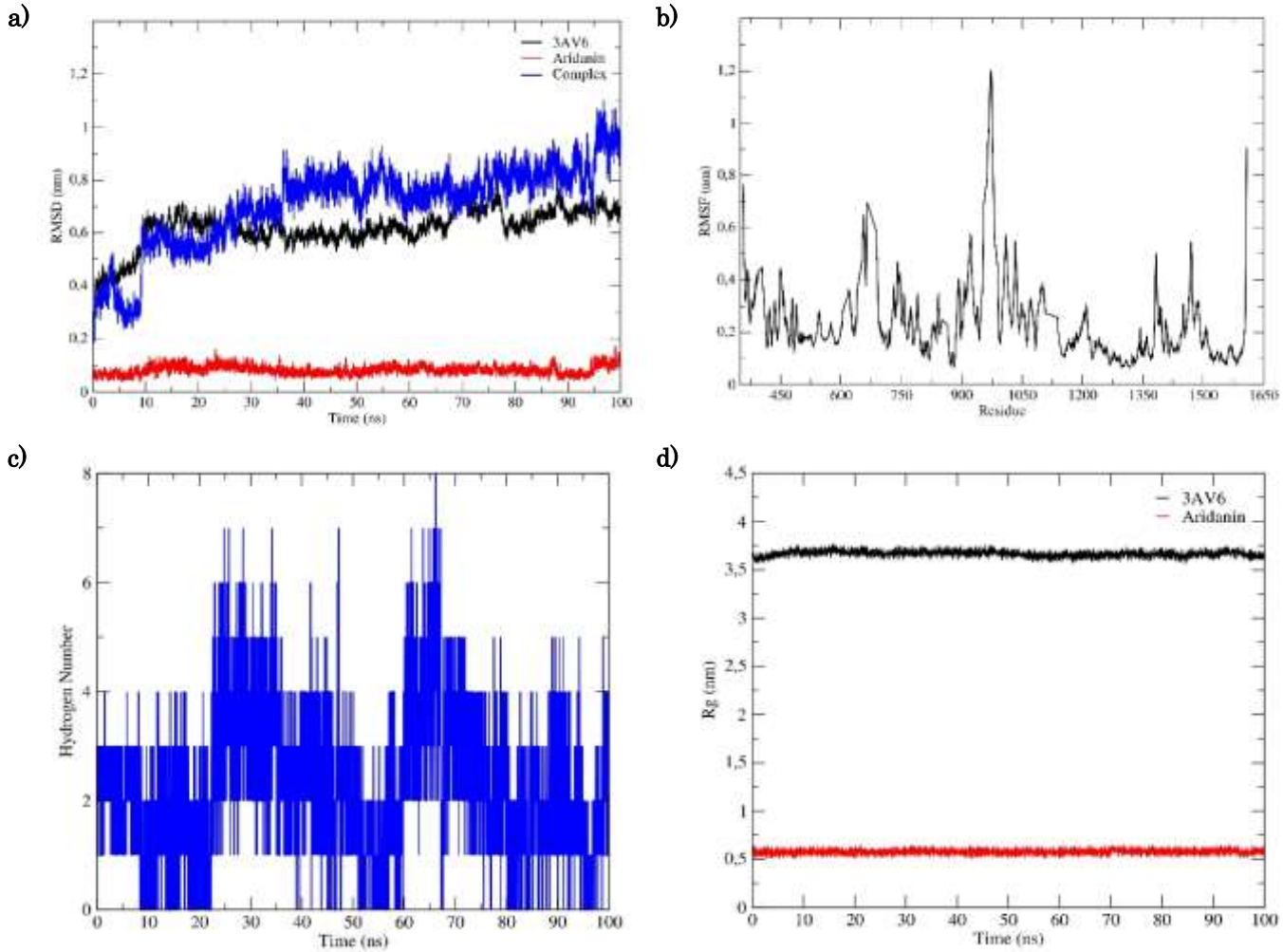

Figure 4. RMSD (a), RMSF (b), time-dependent H-bond interactions (c) and Rg plotting (d) with 3AV6.
Şekil 4. RMSD (a), RMSF (b), zamana bağlı H-bağ etkileşimleri (c) ve 3AV6 ile Rg çizimi (d).

Pharmacokinetic Properties ADMET

Investigating the drug's ADMET characteristics is one of the most important phases in the development of innovative medications. Thus, a molecule that resembles medicine must be absorbed and distributed throughout the body in a sufficient amount and time needed for efficient metabolism (Bruno et al., 2022). The above two physicochemical parameters are complemented by applying Lipinski's "five rules" to the molecule, completing ADMET evaluation (Horchani et al., 2022; Ye et al., 2018). For more information on the extent and strength of the hydrogen bonding process, see the ability of aridanin to donate and accept hydrogen bonds. This improves the interactions and stability of the target enzymes in the active pocket.

Also, the ADMET properties of Aridanin were found to comply and within the norms of Lipinski's "five regimes" (Table 5) except for one rule (molecular weight should be less than 500) when examined by SwissADME. Figure 7 displays aridanin's bioavailability radar graphic, which was retrieved from SwissADME website. The full pinkness of the selected portions, according to (Abdullahi et al., 2022) and (Znati et al., 2019) indicates that aridanin is more pharmacologically friendly and has improved oral bioavailability.

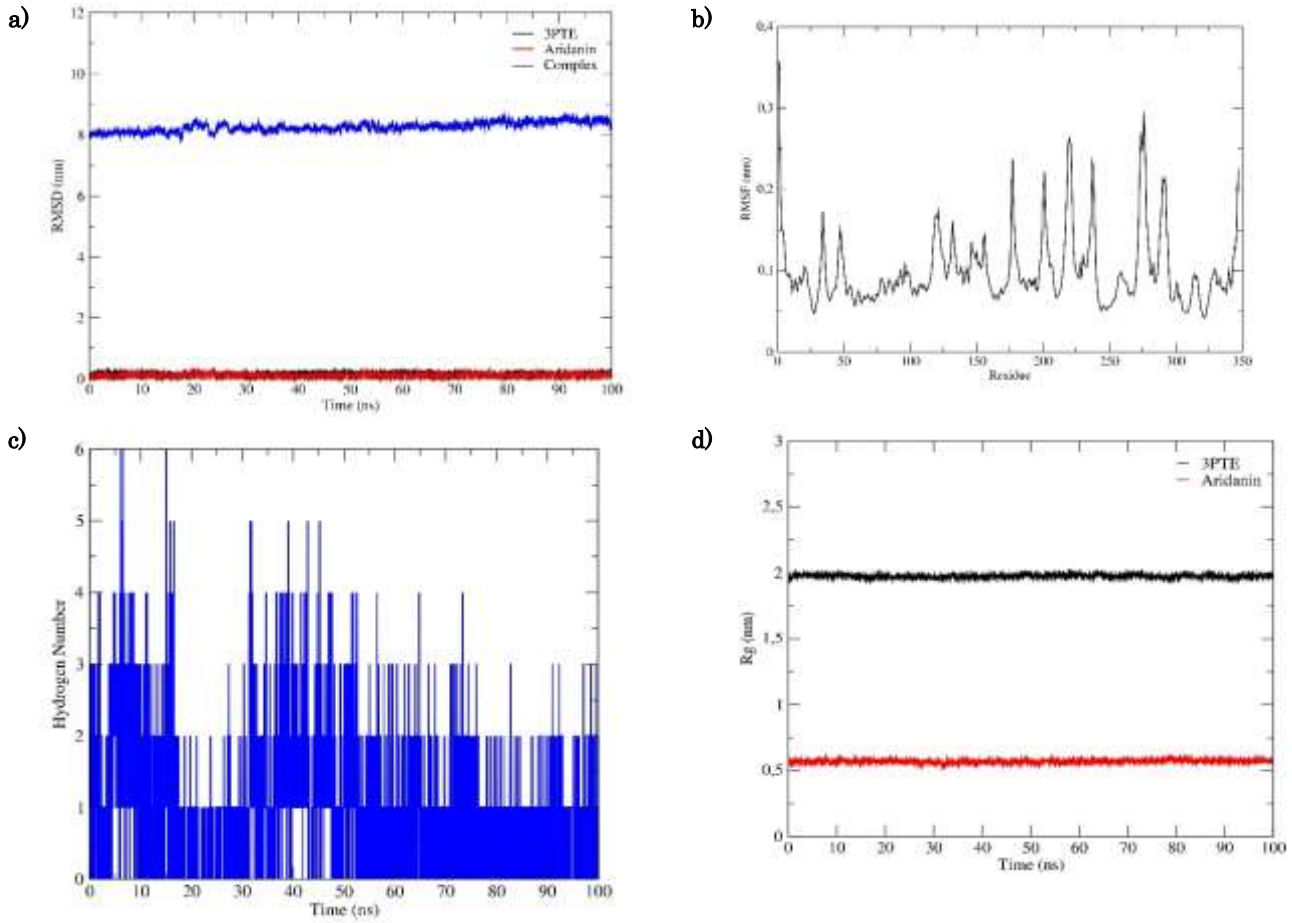

Figure 5. RMSD (a), RMSF (b), time-dependent H-bond interactions (c), and Rg plotting (d) with 3PTE.
Şekil 5. RMSD (a), RMSF (b), zamana bağlı H-bağı etkileşimleri (c) ve 3PTE ile Rg çizimi (d).

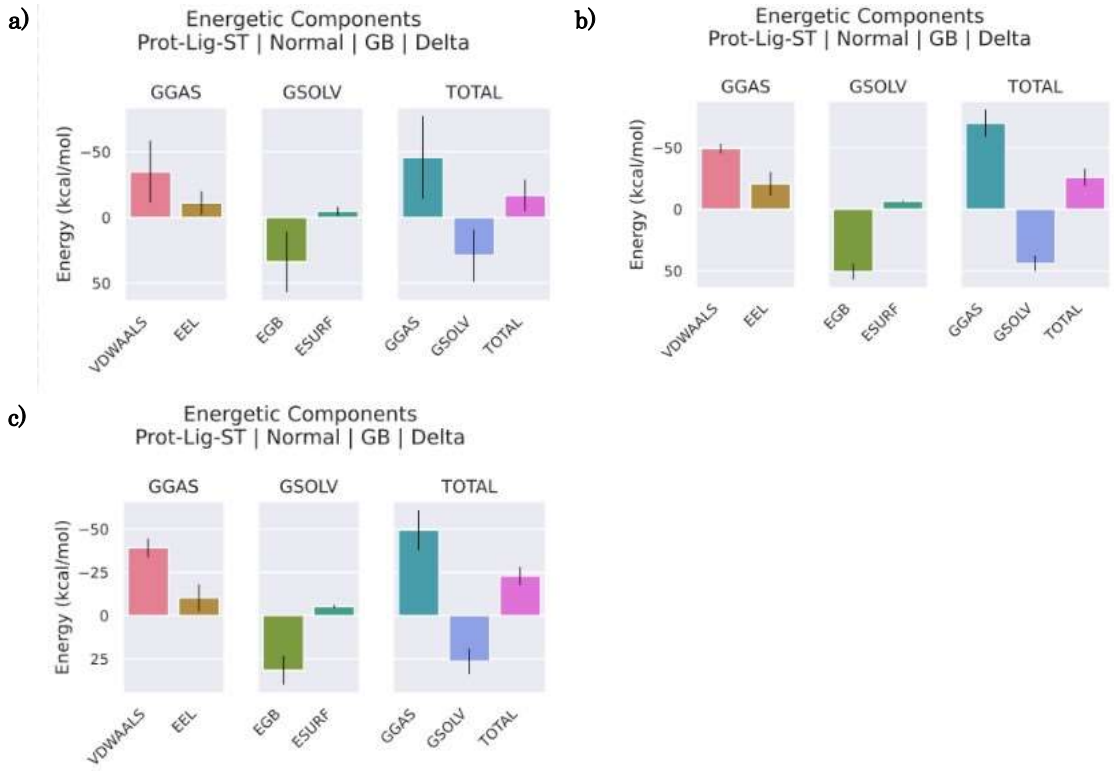

Figure 6. MM-PBSA energy values graphics of 1ZXM (a), 3AV6 (b), and 3PTE (c) with aridanin.
Şekil 6. Aridanin ile 1ZXM (a), 3AV6 (b) ve 3PTE'nin (c) MM-PBSA enerji değerleri grafikleri.

Table 4. Summary results for prediction of activity spectrum of aridanin.
Çizelge 4. Aridaninin aktivite spektrumunun tahmini için özet sonuçları.

No	Pa	Pi	Activity
1	0.991	0.001	Caspase 3 stimulant
2	0.972	0.001	Hepatoprotectant
3	0.968	0.000	Chitinase inhibitor
4	0.945	0.001	Membrane integrity antagonist
5	0.929	0.006	CDP-glycerol glycerophosphotransferase inhibitor
6	0.910	0.001	Caspase 8 stimulant
7	0.912	0.003	Immunostimulant
8	0.903	0.003	Wound healing agent
9	0.900	0.002	Chemopreventive
10	0.897	0.002	Transcription factor NF kappa B stimulant
11	0.897	0.002	Transcription factor stimulant
12	0.883	0.002	Antiviral (Influenza)
13	0.878	0.003	Antiprotozoal (Leishmania)
14	0.835	0.003	Antiulcerative
15	0.831	0.008	Antineoplastic
16	0.826	0.005	Oxidoreductase inhibitor
17	0.820	0.003	Lipid peroxidase inhibitor
18	0.811	0.001	Alpha glucosidase inhibitor
19	0.806	0.002	Antinociceptive
20	0.802	0.001	DNA ligase (ATP) inhibitor
21	0.804	0.008	Apoptosis agonist
22	0.796	0.004	Insulin promoter
23	0.765	0.004	Aspartyl transferase inhibitor
24	0.763	0.004	Hepatic disorders treatment
25	0.696	0.005	Antitoxic
26	0.687	0.010	Antifungal
27	0.692	0.018	Immunosuppressant
28	0.677	0.004	CYP2C9 inducer
29	0.662	0.002	ICAM1 expression inhibitor
30	0.671	0.020	Anti-inflammatory
31	0.657	0.011	Antipruritic
32	0.643	0.004	Nitric oxide antagonist
33	0.673	0.034	Benzoate-CoA ligase inhibitor
34	0.653	0.015	Vasodilator. peripheral
35	0.648	0.018	Hypolipemic
36	0.629	0.002	Phosphorylase inhibitor
37	0.622	0.002	Hyaluronic acid agonist
38	0.621	0.002	Severe acute respiratory syndrome treatment
39	0.620	0.004	Myc inhibitor
40	0.620	0.005	Mannosyl-glycoprotein endo-beta-N-acetylglucosaminidase inhibitor
41	0.603	0.013	Vasodilator
42	0.593	0.005	Alpha-N-acetylglucosaminidase inhibitor
43	0.594	0.009	Antineoplastic (lung cancer)
44	0.637	0.054	CYP2H substrate
45	0.574	0.010	Antibacterial
46	0.579	0.017	Peptide-N4-(N-acetyl-beta-glucosaminyl)asparagine amidase inhibitor
47	0.604	0.045	Phosphatase inhibitor
48	0.584	0.032	Glyceryl-ether monooxygenase inhibitor
49	0.597	0.045	Alkenylglycerophosphocholine hydrolase inhibitor
50	0.567	0.019	Antithrombotic
51	0.563	0.022	Beta glucuronidase inhibitor
52	0.563	0.025	Cholesterol antagonist
53	0.546	0.011	Antimetastatic
54	0.518	0.005	Antineoplastic (melanoma)
55	0.510	0.016	Interleukin 2 agonist
56	0.515	0.024	Lactase inhibitor
57	0.516	0.029	Dermatologic
58	0.501	0.023	Phosphoinositide 5-phosphatase inhibitor

Table 5: Pharmacokinetic properties and drug likeness of aridanin.
Çizelge 5: Aridaninin farmakokinetik özellikleri ve ilaç benzerliği.

Pharmacokinetic parameters	Results
MW (g/mol)	659.91
nHA	8
nHD	5
nRB	6
logP	5.20
logS	-7.25
logKp	-6.14
GIa	Low
BBB_p	No
P-gp	Yes
TPSA	145.55
IA (Human) %	36.14
CL_{tot} (Log mL/min/kg)	-0.09
VD_{ss} (Human) Log L/kg	-1.57
Oral Acute Toxicity (LD_{50})	2.84
CYP substrate	CYP3A4 substrate
Bioavailability Score	0.56

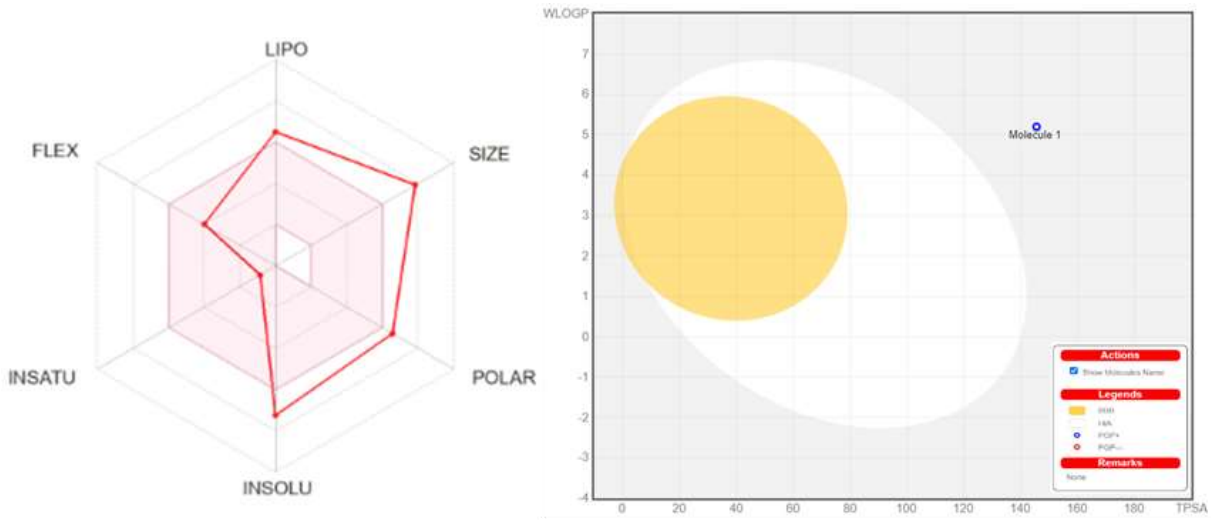

Figure 7. Bioavailability radar chart and Boiled-egg graph of aridanin.
Şekil 7. Aridaninin biyoyararlanım radar grafiği ve haşlanmış yumurta grafiği.

Bioactive chemicals are the best virtual filtration systems because of their pharmacokinetic properties (Bruno et al., 2022). Examination of the boiled egg graph (Figure 7) shows that aridanin has low gastrointestinal absorption (GIa) and no blood-brain barrier permeability (BBBp) because its molecular weight is greater than 500, which should be less than 500 according to Lipinski's rules. Liposomal delivery provides a solution to large molecular weight bioactive molecules that struggle with bioavailability by making them more readily accessible to the body. P-gp is a membrane protein that removes substances from cells. Drugs cannot be P-gp substrates; therefore, the test of aridanin fulfils this condition based on the given estimates. However, CYP (cytochrome P450), which is involved in the oxidative metabolism of drugs, is built on pharmacokinetics-related proteins. Over time, oxidized molecules are eliminated, particularly by the kidneys, due to their polarity. Table 5 demonstrates that aridanin did not interact with CYP isoenzymes, with the exception of the CYP3A4 substrate, highlighting their exceptional capacity to bind second-order toxins (Alminderej et al., 2020; Bruno et al., 2022). This result is in line with the in vitro tests' conclusions on cellular toxicity (Mbaveng et al., 2021). Furthermore, Table 5 indicates that it is more drug-like and advantageous for usage as a medication, with a bioavailability score of 0.56. However, CPY (cytochrome P450), which is involved in the oxidative metabolism of drugs, is built on pharmacokinetics-related proteins. PASS analysis showed that aridanin is capable of exhibiting different biological activities *in vivo*, therefore is a potential candidate for the activities mentioned in Table 4.

Cancer is a leading cause of death worldwide, and even in Africa, which formerly recorded low rates, is witnessing soaring numbers. In 2022, over 20 million new cancer cases and about 10 million deaths were recorded worldwide (Chhikara and Parang, 2022). Projections show that by 2050, the number of new cancer cases per year may rise to 33 million and cancer-related deaths to 18.2 million (Altshuler et al., 2025). In 2019, about 5 million deaths were linked to AMR (Darboe et al., 2022; Kaur et al., 2024; Okeke et al., 2024). Bacterial AMR is growing into an epidemic requiring surveillance, development of drugs with an alternative mechanism of action, as well as implementation of the one health policy (Kim & Cha, 2021; Velazquez-Meza et al., 2022). The spice *T. tetraptera* has recently received wide attention with several research findings establishing aridanin as the major compound (Chi et al., 2024; Gupta, 2022; Kamdem Kengne et al., 2022; K. Sikam et al., 2022; Taiwo et al., 2018; Tang et al., 2022). *T. tetraptera* is an evergreen tree growing in the tropics and subtropics. Its fruit is ever present in the African market and could be a source of antibacterial and anticancer molecules (Bonsou et al., 2022; Chi et al., 2025; Mbaveng et al., 2020). The interest of the present research work was to establish aridanin as an anticancer lead molecule, in line with previous studies which have shown triterpenoids and their saponins as cytotoxic compounds with possible anticancer applications (Fulda, 2008; Gupta, 2022; Ooi et al., 2023). Therefore, aridanin, as a saponin, could be toxic to cancer cells, and even when metabolized to form oleanic acid, the latter still has anticancer properties (Tang et al., 2022). The quantity of aridanin obtained from the fruit of *T. tetraptera* is good enough to fuel initial clinical studies and to some degree the market, while synthetic alternatives could be prepared in the long term.

CONCLUSION

The structure of aridanin, isolated from *T. tetraptera* fruit pulp, was fully determined by analysis of 2D, 3D NMR, HRESIMS, and by comparison to similar data in the literature as 3-*O*-[*β*-D-glucopyranosyl-(2'-acetamido)]-3*β*-olean-12-en-28-oic acid. Molecular docking was used to elucidate the binding modes of aridanin in comparison to doxorubicin towards 6 enzymes involved in cancer metabolism and three bacterial enzymes. The predictions were further confirmed by molecular dynamics simulations on the most active enzymes, together with binding and free energy estimations. Our results showed that aridanin is theoretically a good inhibitor of all six cancer enzymes and three bacterial enzymes, with MolDock scores comparable to the standard drug doxorubicin and binding energies relatively better than the standard. The highest inhibition recorded binding energies of -9.9, -9.2, and -10.9 kcal/mol for topoisomerase II alpha, DNA methyltransferase, and DD-peptidase, respectively. This may suggest that aridanin's anticancer property may be more effective through interference with DNA-related proteins. Equally, we used SwissADME to predict the fate of aridanin in the body and noticed that even though the molecule is drug-like, its gastrointestinal absorption and metabolism are low. Hence requires appropriate drug delivery modeling and further investigations into its elimination. Aridanin could be a more potent anticancer agent in addition to other bioactivities predicted by PASS, and so should be considered for further *in vivo* investigations that could establish it as an anticancer drug candidate.

ACKNOWLEDGMENTS

We acknowledge support from TÜBİTAK through grant no: 3240328525.

We are also thankful to Pr. Dr. Shaheen F. and the ICCBS, where the spectra were recorded.

Contribution Rate Statement Summary of Researchers

The authors declare that they have contributed equally to the article.

Conflict of Interest

The authors declare that there are no known problems that could have an impact on the work described in this manuscript.

REFERENCES

Abdullahi, S. H., Adamu, U., Adamu, S. G., Sani, U., & and Umar, A. B. (2022). Molecular Docking , ADMET and Pharmacokinetic properties predictions of some di-aryl Pyridinamine derivatives as Estrogen Receptor (Er+) Kinase Inhibitors. *Egyptian Journal of Basic and Applied Sciences*, *9*(1), 180-204. https://doi.org/10.1080/2314808X.2022.2050115

Aderibigbe, A., Iwalewa, E. O., Adesina, K. S., & Agboola, I. O. (2011). Anxiolytic effect of aridanin isolated from Tetrapleura tetraptera in mice. *International Journal of Biological and Chemical Sciences*, *4*. https://doi.org/10.4314/ijbcs.v4i5.65523

Adesina, S., Iwalewa, E. O., & Johnny, I. (2016). Tetrapleura tetraptera Taub- Ethnopharmacology, Chemistry,

Medicinal and Nutritional Values- A Review. *British Journal of Pharmaceutical Research*, *12*, 1-22. https://doi.org/10.9734/BJPR/2016/26554

Adesina, S. K., & Reisch, J. (1985). A triterpenoid glycoside from Tetrapleura tetraptera fruit. *Phytochemistry*, *24*(12), 3003-3006. https://doi.org/https://doi.org/10.1016/0031-9422(85)80044-3

Alminderej, F., Bakari, S., Almundarij, T. I., Snoussi, M., Aouadi, K., & Kadri, A. (2020). Antioxidant Activities of a New Chemotype of Piper cubeba L. Fruit Essential Oil (Methyleugenol/Eugenol): In Silico Molecular Docking and ADMET Studies. *Plants (Basel)*, *9*(11). https://doi.org/10.3390/plants9111534

Altshuler, R. D., Minasian, L. M., Schweppe, C. A., & Kadan-Lottick, N. S. (2025). Chemotherapy-induced peripheral neuropathy research: a National Institutes of Health (NIH) grant portfolio analysis (2014-2023). *JNCI Cancer Spectrum*, *9*(3). https://doi.org/10.1093/jncics/pkaf039

Anyamele, T., Onwuegbuchu, P. N., Ugbogu, E. A., & Ibe, C. (2023). Phytochemical composition, bioactive properties, and toxicological profile of Tetrapleura tetraptera. *Bioorganic Chemistry*, *131*, 106288. https://doi.org/10.1016/j.bioorg.2022.106288

Bandyopadhyay, D., Lopez, G., Cantu, S., Balboa, S., Garcia, A., Silva, C., & Valdes, D. (2018). Key Enzymes in Cancer: Mechanism of Action and Inhibition With Anticancer Agents.

Başar, Y., Hosaflıoğlu, İ., & Erenler, R. (2024). Phytochemical analysis of Robinia pseudoacacia flowers and leaf: quantitative analysis of natural compounds and molecular docking application. *Turkish Journal of Biodiversity*, *7*(1), 1-10.

Başar, Y., & Karadağ, M. (2024). Phytochemical Content Analysis of Different Lavandula Officinalis Extracts by LC-ESI-MS/MS and In Silico Molecular Docking Studies. *Turkish Journal of Applied Sciences and Technology*, *5*(1), 12-22. https://doi.org/10.5281/zenodo.11237944

Başar, Y., Yenigün, S., Alma, M. H., Demirtas, İ., & Ozen, T. (2025). Fruit extracts of Rosa canina L. and Rosa pimpinellifolia L.: Phytochemical profiles, in vitro antioxidant, anti-inflammatory, xanthine oxidase inhibitory effects, and in silico molecular dynamics studies. *Kahramanmaraş Sütçü İmam Üniversitesi Tarım ve Doğa Dergisi*, *28*(3), 636-649. https://doi.org/https://doi.org/10.18016/ksutarimdoga.vi.1639294

Bonsou, I. N., Mbaveng, A. T., Nguenang, G. S., Chi, G. F., Kuete, V., & Efferth, T. (2022). Cytotoxicity, acute and sub-chronic toxicities of the fruit extract of Tetrapleura tetraptera (Schumm. & Thonn.) Taub. (Fabaceae). *BMC Complement Med Ther*, *22*(1), 178. https://doi.org/10.1186/s12906-022-03659-1

Brogi, S., Ramalho, T. C., Kuca, K., Medina-Franco, J. L., & Valko, M. (2020). Editorial: In silico Methods for Drug Design and Discovery. *Front Chem*, *8*, 612. https://doi.org/10.3389/fchem.2020.00612

Bruno, S., Bersani, M., Astore, S., Chiabotto, G., Barge, A., Binello, A., & Spyrakis, F. (2022). Lack of interaction of the fluorosurfactant C6O4 with human renal transporters: In vitro/in silico analysis. *Toxicology*, *476*, 153257. https://doi.org/10.1016/j.tox.2022.153257

Chen, C., Lu, L., Yan, S., Yi, H., Yao, H., Wu, D., He, G., Tao, X., & Deng, X. (2018). Autophagy and doxorubicin resistance in cancer. *Anti-Cancer Drugs*, *29*(1), 1-9. https://doi.org/10.1097/cad.0000000000000572

Chhikara, B., & Parang, K. (2022). Global Cancer Statistics 2022: The Trends Projection Analysis. *Chemical Biology Letters*, *10*, 451.

Chi, G. F., Khan, S., Başar, Y., Kuete, J. R. N., Matieta, V. Y., Kuete, J. B. T., Megaptche, J. F., Chongong, M. A., Yenigün, S., Ayimele, G. A., Mbaveng, A. T., Kuete, V., & Shaheen, F. (2025). Antibacterial flavonoids from Tetrapleura tetraptera (Fabaceae) fruit pulp, in silico studies. *South African Journal of Botany*, *180*, 96-106. https://doi.org/https://doi.org/10.1016/j.sajb.2025.02.026

Chi, G. F., Serab, K., N., K. J. R., Y., M. V., O., O. J., N., T. A., F., M. J., A., C. M., B., D. T., Victor, K., & and Shaheen, F. (2024). Triterpenoid saponins from the fruit pulp of Tetrapleura tetraptera (Fabaceae). *Natural Product Research*, 1-13. https://doi.org/10.1080/14786419.2024.2426072

Daina, A., Michielin, O., & Zoete, V. (2017). SwissADME: a free web tool to evaluate pharmacokinetics, drug-likeness and medicinal chemistry friendliness of small molecules. *Scientific Reports*, *7*, 42717. https://doi.org/10.1038/srep42717

Darboe, S., Bradbury, R. S., Phelan, J., Kanteh, A., Muhammad, A.-K., Worwui, A., Yang, S., Nwakanma, D., Perez-Sepulveda, B., & Kariuki, S. (2022). Genomic diversity and antimicrobial resistance among non-typhoidal Salmonella associated with human disease in The Gambia. *Microbial Genomics*, *8*(3), 000785. https://doi.org/https://doi.org/10.1099/mgen.0.000785

Decherchi, S., & Cavalli, A. (2020). Thermodynamics and Kinetics of Drug-Target Binding by Molecular Simulation. *Chem Rev*, *120*(23), 12788-12833. https://doi.org/10.1021/acs.chemrev.0c00534

Elkaeed, E. B., Yousef, R. G., Elkady, H., Gobaara, I. M. M., Alsfouk, B. A., Husein, D. Z., Ibrahim, I. M., Metwaly, A. M., & Eissa, I. H. (2022). Design, Synthesis, Docking, DFT, MD Simulation Studies of a New Nicotinamide-Based Derivative: In Vitro Anticancer and VEGFR-2 Inhibitory Effects. *Molecules*, *27*(14), 4606. https://www.mdpi.com/1420-3049/27/14/4606

Espinosa, E., Zamora, P., Feliu, J., & González Barón, M. (2003). Classification of anticancer drugs--a new system based on therapeutic targets. *Cancer Treatment Reviews*, *29*(6), 515-523. https://doi.org/10.1016/s0305-7372(03)00116-6

Fulda, S. (2008). Betulinic Acid for Cancer Treatment and Prevention. *International Journal of Molecular Sciences*, *9*(6), 1096-1107. https://www.mdpi.com/1422-0067/9/6/1096

Gok, M., Basar, Y., Yenigun, S., Ipek, Y., Behcet, L., Ozen, T., & Demirtas, I. (2025). Bioactive Apigenin-7-O-ß-Glucoside and Rosmarinic Acid Molecules From Two Nepeta Species: Bioactivity-Guided Isolation, In Vitro Evaluations, Pharmacokinetic and In Silico Approaches as Metabolic Enzyme Inhibition Agents. *Phytochemical Analysis*. https://doi.org/https://doi.org/10.1002/pca.3536

Gupta, N. (2022). A review on recent developments in the anticancer potential of oleanolic acid and its analogs (2017-2020). *Mini Reviews in Medicinal Chemistry*, *22*(4), 600-616. https://doi.org/10.2174/1389557521666210810153627

Hafezi, S., & Rahmani, M. (2021). Targeting BCL-2 in Cancer: Advances, Challenges, and Perspectives. *Cancers*, *13*(6), 1-15. https://doi.org/10.3390/cancers13061292

Horchani, M., Heise, N. V., Csuk, R., Ben Jannet, H., Harrath, A. H., & Romdhane, A. (2022). Synthesis and In Silico Docking Study towards M-Pro of Novel Heterocyclic Compounds Derived from Pyrazolopyrimidinone as Putative SARS-CoV-2 Inhibitors. *Molecules*, *27*(16). https://doi.org/10.3390/molecules27165303

İpek, Y., Yunus, B., Semiha, Y., Lütfi, B., Tevfik, Ö., & and Demirtaş, İ. In vitro bioactivities and in silico enzyme interactions of abietatrien-3ß-ol by bio-guided isolation from Nepeta italica subsp. italica. *Journal of Biomolecular Structure and Dynamics*, 1-24. https://doi.org/10.1080/07391102.2024.2322626

Kamdem Kengne, M. H., Gertrude Laura, F., Silihe, K., More, G., Mphahlele, M., Moswetsa, T., Tata, C., Tonga, J., Ojo, O., Thierry, F., Mmutlane, E., & Ndinteh, D. (2022). Cytotoxic and antibacterial activities of compounds isolated from the fruits and stem-bark of Tetrapleura tetraptera (Schumach. & Thonn.) Taub. (Fabaceae). *Medicinal Chemistry Research*, *31*. https://doi.org/10.1007/s00044-022-02956-1

Kaur, J., Singh, H., & Sethi, T. (2024). Emerging trends in antimicrobial resistance in bloodstream infections: multicentric longitudinal study in India (2017–2022). *The Lancet Regional Health - Southeast Asia*, *26*. https://doi.org/10.1016/j.lansea.2024.100412

Kim, D. W., & Cha, C. J. (2021). Antibiotic resistome from the One-Health perspective: understanding and controlling antimicrobial resistance transmission. *Exp Mol Med*, *53*(3), 301-309. https://doi.org/10.1038/s12276-021-00569-z

Kohanski, M. A., Dwyer, D. J., & Collins, J. J. (2010). How antibiotics kill bacteria: from targets to networks. *Nature Reviews: Microbiology*, *8*(6), 423-435. https://doi.org/10.1038/nrmicro2333

Kumar, S., Ahmad, M., Waseem, M., & Pandey, A. K. (2015). Drug Targets for Cancer Treatment: An Overview. *Medicinal Chemistry*, *5*. https://doi.org/10.4172/2161-0444.1000252

Kumari, R., Kumar, R., Consortium, O. S. D. D., & Lynn, A. (2014). g_mmpbsa□ A GROMACS tool for high-throughput MM-PBSA calculations. *Journal of chemical information and modeling*, *54*(7), 1951-1962.

Lagunin, A., Stepanchikova, A., Filimonov, D., & Poroikov, V. (2000). PASS: prediction of activity spectra for biologically active substances. *Bioinformatics*, *16*(8), 747-748. https://doi.org/10.1093/bioinformatics/16.8.747

Lao, J., Madani, J., Puértolas, T., Alvarez, M., Hernández, A., Pazo-Cid, R., Artal, A., & Antón Torres, A. (2013). Liposomal Doxorubicin in the treatment of breast cancer patients: a review. *J Drug Deliv*, *2013*, 456409. https://doi.org/10.1155/2013/456409

Lin, J. H. (2016). Review structure- and dynamics-based computational design of anticancer drugs. *Biopolymers*, *105*(1), 2-9. https://doi.org/10.1002/bip.22744

Liu, X., Shi, D., Zhou, S., Liu, H., Liu, H., & Yao, X. (2018). Molecular dynamics simulations and novel drug discovery. *Expert Opin Drug Discov*, *13*(1), 23-37. https://doi.org/10.1080/17460441.2018.1403419

Majewski, M., Ruiz Carmona, S., & Barril, X. (2019). An investigation of structural stability in protein-ligand complexes reveals the balance between order and disorder. *Communications Chemistry*, *2*, 1-8. https://doi.org/10.1038/s42004-019-0205-5

Marvalim, C., Datta, A., & Lee, S. C. (2023). Role of p53 in breast cancer progression: An insight into p53 targeted therapy. *Theranostics*, *13*(4), 1421-1442. https://doi.org/10.7150/thno.81847

Mbaveng, A. T., Chi, G. F., Bonsou, I. N., Abdelfatah, S., Tamfu, A. N., Yeboah, E. M. O., Kuete, V., & Efferth, T. (2020). N-acetylglycoside of oleanolic acid (aridanin) displays promising cytotoxicity towards human and animal cancer cells, inducing apoptotic, ferroptotic and necroptotic cell death. *Phytomedicine*, *76*, 153261. https://doi.org/10.1016/j.phymed.2020.153261

Mbaveng, A. T., Chi, G. F., Bonsou, I. N., Ombito, J. O., Yeboah, S. O., Kuete, V., & Efferth, T. (2021). Cytotoxic phytochemicals from the crude extract of Tetrapleura tetraptera fruits towards multi-factorial drug resistant cancer cells. *J Ethnopharmacol*, *267*, 113632. https://doi.org/10.1016/j.jep.2020.113632

Meredith, A. M., & Dass, C. R. (2016). Increasing role of the cancer chemotherapeutic doxorubicin in cellular metabolism. *Journal of Pharmacy and Pharmacology*, *68*(6), 729-741. https://doi.org/10.1111/jphp.12539

Micallef, I., & Baron, B. (2020). Doxorubicin: An Overview of the Anti-Cancer and Chemoresistance Mechanisms OPEN ACCESS. *3*, 1031.

Namba-Nzanguim, C. T., Simoben, C. V., Bekono, B. D., Tietjen, I., Cassel, J., Salvino, J. M., Montaner, L. J., Davis, R. A., & Ntie-Kang, F. (2024). Investigation of some plant stilbenoids and their fragments for the identification of inhibitors of SARS-CoV-2 viral spike/ACE2 protein binding. *The Microbe*, *3*, 100059. https://doi.org/https://doi.org/10.1016/j.microb.2024.100059

Okeke, I. N., de Kraker, M. E. A., Van Boeckel, T. P., Kumar, C. K., Schmitt, H., Gales, A. C., Bertagnolio, S., Sharland, M., & Laxminarayan, R. (2024). The scope of the antimicrobial resistance challenge. *The Lancet*, *403*(10442), 2426-2438. https://doi.org/10.1016/S0140-6736(24)00876-6

Ooi, K. X., Poo, C. L., Subramaniam, M., Cordell, G. A., & Lim, Y. M. (2023). Maslinic acid exerts anticancer effects by targeting cancer hallmarks. *Phytomedicine*, *110*, 154631. https://doi.org/10.1016/j.phymed.2022.154631

Qian, S., Wei, Z., Yang, W., Huang, J., Yang, Y., & Wang, J. (2022). The role of BCL-2 family proteins in regulating apoptosis and cancer therapy. *Frontiers in Oncology*, *12*, 985363. https://doi.org/10.3389/fonc.2022.985363

Rapaport, D. (2004). The Art of Molecular Dynamics Simulaton. *The Art of Molecular Dynamics Simulation*. https://doi.org/10.1017/CBO9780511816581

Rehman, M. T., AlAjmi, M. F., Hussain, A., Rather, G. M., & Khan, M. A. (2019). High-Throughput Virtual Screening, Molecular Dynamics Simulation, and Enzyme Kinetics Identified ZINC84525623 as a Potential Inhibitor of NDM-1. *International Journal of Molecular Sciences*, *20*(4). https://doi.org/10.3390/ijms20040819

Siegel, R. L., Miller, K. D., Wagle, N. S., & Jemal, A. (2023). Cancer statistics, 2023. *CA: A Cancer Journal for Clinicians*, *73*(1), 17-48. https://doi.org/10.3322/caac.21763

Sikam, K., Ntabo, V., Happi, G., Meikeu, L., & Wansi, J. (2022). Chemistry and pharmacological aspects of Aridanin, a lead compound from Tetrapleura tetraptera (Fabaceae). *Natural Resources for Human Health*, *3*. https://doi.org/10.53365/nrfhh/152273

Sikam, K. G., Happi, G. M., Ahmed, S. A., Wakeu, B. N. K., Meikeu, L. Z., Salau, S., & Wansi, J. D. (2022). In vitro antiplasmodial, molecular docking and pharmacokinetics studies of specialized metabolites from Tetrapleura tetraptera (Fabaceae). *South African Journal of Botany*, *151*, 949-959. https://doi.org/https://doi.org/10.1016/j.sajb.2022.11.021

Spencer, A. C., & Panda, S. S. (2023). DNA Gyrase as a Target for Quinolones. *Biomedicines*, *11*(2). https://doi.org/10.3390/biomedicines11020371

Taiwo, B. J., Olubiyi, O. O., Wang, X., Fisusi, F. A., Akinniyi, G. A., Van Heerden, F. R., & Strodel, B. (2018). Schistosomiasis: Snail-vector control, molecular modelling and dynamic studies of bioactive N-acetylglycoside saponins from Tetrapleura tetraptera. *Comput Biol Chem*, *77*, 363-372. https://doi.org/10.1016/j.compbiolchem.2018.09.011

Tang, Z.-Y., Li, Y., Tang, Y.-T., Ma, X.-D., & Tang, Z.-Y. (2022). Anticancer activity of oleanolic acid and its derivatives: Recent advances in evidence, target profiling and mechanisms of action. *Biomedicine and Pharmacotherapy*, *145*, 112397. https://doi.org/https://doi.org/10.1016/j.biopha.2021.112397

Velazquez-Meza, M. E., Galarde-López, M., Carrillo-Quiróz, B., & Alpuche-Aranda, C. M. (2022). Antimicrobial resistance: One Health approach. *Vet World*, *15*(3), 743-749. https://doi.org/10.14202/vetworld.2022.743-749

Wang, W., Albadari, N., Du, Y., Fowler, J. F., Sang, H. T., Xian, W., McKeon, F., Li, W., Zhou, J., & Zhang, R. (2024). MDM2 Inhibitors for Cancer Therapy: The Past, Present, and Future. *Pharmacological Reviews*, *76*(3), 414-453. https://doi.org/10.1124/pharmrev.123.001026

WHO. (2024). *WHO bacterial priority pathogens list, 2024: bacterial pathogens of public health importance, to guide research, development, and strategies to prevent and control antimicrobial resistance*. World Health Organization.

Wojciechowski, M., Milewski, S., Mazerski, J., & Borowski, E. (2005). Glucosamine-6-phosphate synthase, a novel target for antifungal agents. Molecular modelling studies in drug design. *Acta Biochimica Polonica*, *52*(3), 647-653.

Ye, F., Ma, P., Zhang, Y. Y., Li, P., Yang, F., & Fu, Y. (2018). Herbicidal Activity and Molecular Docking Study of Novel ACCase Inhibitors. *Frontiers of Plant Science*, *9*, 1850. https://doi.org/10.3389/fpls.2018.01850

Yenigun, S., Yunus, B., Yasar, I., Lutfi, B., Ibrahim, D., & and Ozen, T. (2024a). Comprehensive evaluation of Ixoroside: An iridoid glycoside from Nepeta aristata and N. baytopii, assessing antioxidant, antimicrobial, enzyme inhibitory, DNA protective properties, with computational and pharmacokinetic analyses. *Journal of Biologically Active Products from Nature*, *14*(3), 286-315. https://doi.org/10.1080/22311866.2024.2358785

Yenigun, S., Yunus, B., Yasar, I., Lutfi, B., Ibrahim, D., & and Ozen, T. (2024b). DNA protection, molecular docking, molecular dynamic, enzyme inhibition, and kinetics studies of apigenin isolated from Nepeta baytopii Hedge & Lamond by bioactivity-guided fractionation. *Journal of Biomolecular Structure and Dynamics*, 1-12.

https://doi.org/10.1080/07391102.2024.2442753

Yenigün, S., Başar, Y., Yılmaz, S., Demirtas, İ., & Ozen, T. (2024c). Phytochemical Contents and Antioxidant Activity Paliurus Spina-Christi Miller Leaf and Seed Extracts: PASS Predictions, In Silico Studies on Xanthine Oxidase and Cytochrome P450 1A1. *Current Perspectives on Medicinal and Aromatic Plants*, *7*(2), 96-106. https://doi.org/10.38093/cupmap.1516991

Yoshino, T., Shiina, H., Urakami, S., Kikuno, N., Yoneda, T., Shigeno, K., & Igawa, M. (2006). Bcl-2 expression as a predictive marker of hormone-refractory prostate cancer treated with taxane-based chemotherapy. *Clin Cancer Res*, *12*(20 Pt 1), 6116-6124. https://doi.org/10.1158/1078-0432.Ccr-06-0147

Yousef, R. G., Albaraa, I., M., K. M., M., E. W., M., G. I. M., M., M. A. B., B., E. E., A., A. A., M., M. A., & and Eissa, I. H. (2022). Discovery of new nicotinamides as apoptotic VEGFR-2 inhibitors: virtual screening, synthesis, anti-proliferative, immunomodulatory, ADMET, toxicity, and molecular dynamic simulation studies. *Journal of Enzyme Inhibition and Medicinal Chemistry*, *37*(1), 1389-1403. https://doi.org/10.1080/14756366.2022.2070744

Zhang, C., Wang, X., Du, J., Gu, Z., & Zhao, Y. (2021). Reactive Oxygen Species-Regulating Strategies Based on Nanomaterials for Disease Treatment. *Adv Sci (Weinh)*, *8*(3), 2002797. https://doi.org/10.1002/advs.202002797

Zhang, Z., Wang, G., Li, Y., Lei, D., Xiang, J., Ouyang, L., Wang, Y., & Yang, J. (2022). Recent progress in DNA methyltransferase inhibitors as anticancer agents. *Frontiers in Pharmacology*, *13*, 1072651. https://doi.org/10.3389/fphar.2022.1072651

Zhao, Y., Yu, H., & Hu, W. (2014). The regulation of MDM2 oncogene and its impact on human cancers. *Acta Biochim Biophys Sin (Shanghai)*, *46*(3), 180-189. https://doi.org/10.1093/abbs/gmt147

Zheng, K., Dong, Y., Yang, R., Liang, Y., Wu, H., & He, Z. (2021). Regulation of ferroptosis by bioactive phytochemicals: Implications for medical nutritional therapy. *Pharmacological Research*, *168*, 105580. https://doi.org/10.1016/j.phrs.2021.105580

Znati, M., Bordes, C., Forquet, V., Lantéri, P., Ben Jannet, H., & Bouajila, J. (2019). Synthesis, molecular properties, anti-inflammatory and anticancer activities of novel 3-hydroxyflavone derivatives. *Bioorganic Chemistry*, *89*, 103009. https://doi.org/10.1016/j.bioorg.2019.103009 .